DOES THE GROWTH HORMONE-DERIVED PEPTIDE AOD9604 HAVE AN ANABOLIC EFFECT ON BONE?

by

Ivan Kamikovski

A thesis submitted in conformity with the requirements
for the degree of Master of Applied Science
Graduate Department of the Institute of Biomaterials and Biomedical Engineering
University of Toronto

Your file Votre référence
ISBN: 978-0-494-52651-4
Our file Notre référence
ISBN: 978-0-494-52651-4

Abstract

Does the Growth Hormone-Derived Peptide AOD9604 have an Anabolic Effect on Bone?

Ivan Kamikovski
Master of Applied Science
Institute of Biomaterials and Biomedical Engineering
University of Toronto
2009

This study focused on the ability of AOD to rebuild the bone lost during ovariectomy (OVX) in a rat model of postmenopausal osteoporosis. Bone quality was evaluated through densitometry, mechanical testing, and techniques to assess remodeling, structural and material properties.

We found that the anabolic effect of AOD was dose-dependent and site-specific. In cortical bone, AOD increased the cross-section of the femoral diaphysis via periosteal apposition without much effect on mechanical properties. In trabecular bone, AOD partially restored trabecular architecture, which resulted in an improvement in vertebral mechanical properties. In addition, AOD increased mineralization as well as stiffness and modulus of cortical and trabecular bone indicating that AOD may also have some anti-resorptive effect in addition to its anabolic effect.

Acknowledgements

I would like to take this opportunity to gratefully acknowledge the kind support offered to me by my mentors and colleagues throughout the duration of this project. Foremost amongst these is my supervisor, Dr. Marc Grynpas, to whom I am thankful for his guidance in both the design and execution of this study. I would also like to acknowledge my committee members, Dr. Rita Kandel and Dr. Eli Sone, for their helpful suggestions and careful edits.

This work would not have been completed without technical assistance. I would like to thank Dr. Richard Renlund who had a large part in the study design and the care and treatment of the animals. I am also thankful to Dr. Mircea Dumitriu for his valuable help in obtaining data for mineralization profiles and connectivity of proximal tibiae, to Mr. Douglas Holmyard for his assistance in scanning electron microscopy, and to Mrs. Maria Mendez for her valuable help in histomorphometry.

I would also like to acknowledge the members of the Grynpas lab. I would especially like to thank Mr. Richard Cheung, the laboratory manager, for being so efficient and attentive, Dr. Thomas Willett for his expertise in mechanical engineering, and Dr. Herman Thang for his support and advice in both professional and other matters

On a personal note, I would like to thank my father and my mother, for their support and encouragement during the entire duration of this study. I am grateful to my brother for sharing a lot of my burdens and lighting up moments of stress. Last, but certainly not least, I am thankful to Andra for being a pillar of support and strength and for continually reminding me that through hard work and dedication, anything is possible.

Table of Contents

List of Tables

List of Figures

List of Abbreviations

AOD	anti-obesity drug
β3-AR	β3-adrenergic receptor
BMC	bone mineral content
BMD	bone mineral density
BMU	bone multicellular unit
BSP	bone sialoprotein
DXA	Dual energy x-ray absorptiometry
ES	eroded surface
GHBP	Growth Hormone binding protein
GHR	Growth Hormone receptor
GHRH	Growth Hormone-releasing hormone
hGH	human Growth Hormone
GLUT 4	glucose-transporter 4
IGF-I	Insulin-like growth factor
NC	normal control
OC	OVX control
O.Th.	osteoid thickness
OS	osteoid surface
OS/BS	osteoid surface (percentage of bone surface)
OV	osteoid volume
OVX	ovariectomy
PMMA	polymethylmethacrylate
PTH	parathyroid hormone
qBSE	quantitative back scattered electron
SEM	scanning electron microscope
SERM	selective estrogen receptor modulator
Tb.N.	trabecular number
Tb.Sp.	trabecular separation
Tb.Th.	trabecular thickness
TRAP	Tartrate-Resistant Acid Phosphatase
TBV	trabecular bone volume
TV	tissue volume

Chapter 1 : Introduction and Background

1 Introduction

Obesity has become an increasing problem globally and especially in North America where 47.9% of Canadians were overweight in 1997 (MacDonald *et al.*, 1997). Furthermore, obesity causes a significant strain on the healthcare system since it increases the risk of many diseases including heart disease, diabetes and many types of cancers (MacDonald *et al.*, 1997).

Growth hormone (GH), a peptide hormone secreted from the anterior pituitary, is mainly known for its stimulatory effect on longitudinal bone growth but it also stimulates fat metabolism. The use of GH for the treatment of human obesity has not been advocated due to serious side effects, including glucose intolerance, insulin resistance, sodium retention, hypertension, edema, and carpal tunnel syndrome (Daughaday and Harvey, 1994)

It was discovered that the domain of GH responsible for lipid metabolism is located at the carboxy-terminal end of the molecule (Ng *et al.*, 2000). Peptide hGH(177-191), now called AOD9604, has been synthesized and has similar lipolytic activities as intact hGH without any diabetogenic side effects (Heffernan *et al.*, 2001b; Heffernan *et al.*, 2001a; Ng *et al.*, 2000).

Since GH is anabolic to the skeleton, it is important to understand if this skeletal effect is conserved in AOD9604.

The present study will determine if AOD can act *in vivo* to rebuild the bone lost during ovariectomy (OVX) in a rat model of postmenopausal osteoporosis. This model of increased turnover activity will allow subtle changes to be amplified and more readily observed. Bone quality will be determined by assessment of parameters including bone mineral density, bone mechanical properties, bone mineralization, bone architecture, and bone remodeling (formation and resorption).

1.1 Bone Biology

The skeletal system serves many physiological purposes. Its numerous functions include acting as a reservoir for minerals such as calcium, physical protection for vital internal organs, and provision of a framework that allows skeletal motion. From a biomechanical standpoint, bone is a complex engineering material that has been designed to function across a wide range of loading. Before the biomechanical complexity of bone can be discussed, it is necessary to have a general knowledge of bone biology: its underlying composition, the dynamic nature of bone remodeling, and the various types of bones that make up our skeleton.

1.1.1 Composition

Bone is a complex composite material consisting of two main phases: a mineral phase embedded within a compliant organic matrix. Bone consists of approximately 65% mineral and 35% organic matrix, including proteins, cells and water (Jee, 2001). The mineral component of bone is formed by small, impure, poorly crystalline and highly substituted hydroxyapatite crystals ($Ca_{10}(PO_4)_6(OH)_2$). The mineral phase largely contributes to the overall strength and stiffness of bone. In human bone, the apatite is present as a plate-like crystal, which is 20 to 80 nm long and 2 to 5 nm thick (Kaplan *et al.*, 1994).

The organic matrix consists mainly (~ 90%) of Type I collagen; the remainder consists of noncollagenous matrix proteins, minor collagen types, lipids, and other macromolecules. Collagen is a ubiquitous protein, which consists of three polypeptide chains composed of approximately 1000 amino acids each. It is the major structural component of the bone matrix. Bone collagen is constructed in the form of a triple helix of two identical $\alpha 1$ chains and one unique $\alpha 2$ chain cross-linked by hydrogen bonding between hydroxyproline and other charged residues. This produces a fairly rigid linear molecule 300 nm long. Each molecule is aligned

with the next in a parallel fashion in a quarter-staggered array to produce a collagen fibril. The collagen fibrils are then grouped in bundles to form the collagen fiber. Within the collagen fibril, gaps, called "hole zones" exist between the ends of the molecules. Mineralization of the matrix is thought to commence in the hole zones (Kaplan *et al.*, 1994) (Figure 1-1).

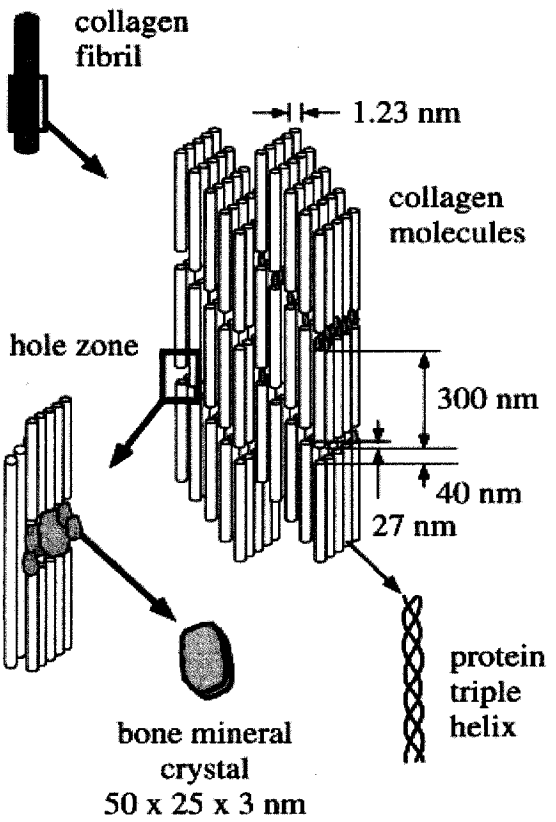

Figure 1-1: A schematic diagram illustrating the assembly of collagen fibrils and fibers and bone mineral crystals (Rho et al., 1998)

1.1.2 Bone Remodeling

The ratio of mineral and organic phases of bone is maintained through a dynamic process known as bone remodeling or turnover. The cellular system by which this process is governed is known as a bone multicelluar unit (BMU). A BMU consist of a group of all the linked cells

that participate in remodeling a certain area of bone through a sequence of cell activity consisting of activation, resorption, reversal, formation, and mineralization (Figure 1-2).

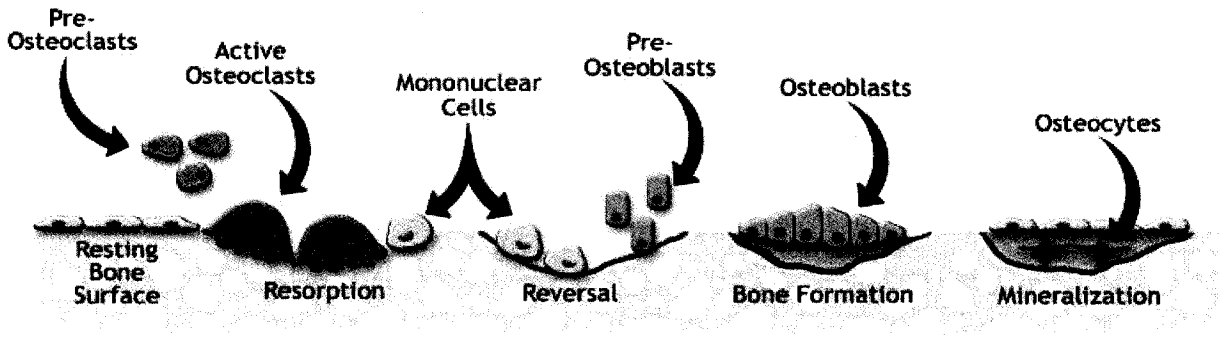

Figure 1-2: Bone remodeling cycle (Newine, 2005)

The first stage of bone remodeling is bone **resorption**, led by active osteoclast cells. Osteoclasts are characterized by their large size (20 to 100 μm in diameter) and their multiple nuclei (Kaplan *et al.*, 1994). These cells are derived from pluripotent cells of the bone marrow, which are the hematopoietic precursors that also give rise to monocytes and macrophages. Once activated osteoclasts resorb old bone through two mechanisms. The mineral phase is dissolved by secretion of hydrogen ions (H+) which increases the solubility of the hydroxyapatite crystals while the organic components of the matrix are removed by acidic proteolytic digestion (Kaplan *et al.*, 1994).

Once the resorption pit is complete, osteoblasts are recruited. These are the bone forming cells, and are rectangular in shape. The cytoplasm of the cell is occupied by three major components; the nucleus, the Golgi apparatus, and the rough endoplasmic reticulum. The nucleus in the osteoblast is large relative to that in other cell types. Osteoblasts originate from a mesenchymal lineage (Kaplan *et al.*, 1994). A resting osteoblast is referred to as a lining cell,

and is initially recruited to line the resorption pit during the **reversal** stage. Next, active osteoblasts are recruited to begin early **bone formation**. In this stage, osteoblasts deposit unmineralized collagenous bone matrix, which is also known as osteoid (Jee, 2001). Several noncollagenous proteins are then involved in the initiation of late bone formation, or the **mineralization** stage. In this later stage, mature osteoblasts are signalled to deposit mineral, the pattern and amount being governed by the organization of the underlying organic matrix (Jee, 2001). In human bone, osteoid experiences 70% of its final mineralization after about 5-10 days (Jee, 2001).

After the majority of the osteoid is mineralized, the final stage, known as **quiescence**, is reached. At any given time, the majority of bone surfaces are at this quiescent or resting stage in the bone remodeling cycle (Jee, 2001). At this stage, inactive osteoblasts can advance into three different fates. First, inactive osteoblasts may remain as lining cells on quiescent bone surfaces. Secondly, inactive osteoblasts may undergo apoptosis, or programmed cell death. Finally, osteoblasts can become embedded within the new bone matrix, after which they are referred to as osteocytes. Osteocytes are the most abundant cell type in mature bone. The metabolic/structural role of osteocytes has not been identified, but their intricate 3-D distribution and their interconnecting cell processes indicate that they are perfectly organized to serve as an intricate system to help communicate strain and stress signals and regulate the overall metabolism of the tissue (Kaplan *et al.*, 1994).

During the quiescent phase, additional mineralization can occur. This additional stage is known as secondary mineralization, and is responsible for the mineralization of the remaining 30% of the osteoid (Jee, 2001). Compared to the initial primary mineralization, this stage takes approximately 3-6 months to complete (Jee, 2001). Governed by mature osteoblasts, secondary

mineralization involves both the deposition of new bone crystals and the continued growth of existing crystals.

1.1.3 Types of Bone

At the microscopic level, bone consists of two forms: woven and lamellar. Woven bone is considered immature bone, or primitive bone, and is normally found in the embryo and the newborn, in fracture callus, and in the metaphyseal region of growing bone (Kaplan *et al.*, 1994). Woven bone is coarse-fibered and contains no uniform orientation of the collagen fibers. It has more cells per unit volume than lamellar bone, its mineral content varies, and its cells are randomly arranged. The relatively disoriented collagen fibers of woven bone give it isotropic mechanical characteristics; when tested, the mechanical behaviour of woven bone is similar regardless of the orientation of the applied forces (Turner and Burr, 2001; Jee, 2001).

Lamellar bone begins to form one month after birth. By 1 year of age, it is actively replacing woven bone, as the latter is resorbed (Kaplan *et al.*, 1994). By age 4, most normal bone is lamellar bone (Kaplan *et al.*, 1994). Lamellar bone is thus more mature bone that results from remodeling of woven or previously existing bone. The highly organized, stress oriented collagen of lamellar bone gives it anisotropic properties; that is, the mechanical behaviour of lamellar bone differs depending on the orientation of the applied forces, with is greatest strength parallel to the longitudinal axis of collagen fibers (Turner and Burr, 2001).

Lamellar bone is structurally organized into trabecular (spongy or cancellous) bone and cortical (dense or compact) bone. Cortical bone has four times the mass of trabecular bone, although the metabolic turnover of trabecular bone is eight times greater than that of cortical bone (Jee, 2001). Bone remodeling is a surface event, and trabecular bone has a greater surface area than cortical bone.

Cortical bone is found as the "envelope" in cuboid bones such as vertebrae, and it composes the diaphysis in long bones (Kaplan *et al.*, 1994). Cortical bone is subject to bending and torsional forces as well as to compressive forces. In humans, cortical bone is organized into Haversian systems, which are cylindrical units surrounding a central vascular canal (Haversian canal). These canals, and the corresponding concentric layers, lie parallel to the length of the bone. A single cylindrical unit is known as an osteon, and numerous osteons are then organized to form cortical bone (Jee, 2001). It should be noted that while many mammals possess Haversian systems in their cortical bone, others do not. In particular, rodents such as rats do not possess Haversian systems under natural conditions (Kalu, 1991).

Trabecular bone is found principally at the metaphysis and epiphysis of long bones and in cuboid bones (Jee, 2001). The internal beams or spicules of trabecular bone form a three-dimensional branching lattice aligned along the lines of stress. Because of its relatively high remodeling rate, trabecular bone is typically more affected by dysfunctions in bone remodeling.

1.2 Postmenopausal Osteoporosis

Osteoporosis is a multifactorial, age-related metabolic bone disease characterized by low bone mineral density, the deterioration of the microarchitecture of trabecular bone, and changes in the material properties of bone, leading to enhanced bone fragility and to a consequent increase in the risk of fracture (Grynpas *et al.*, 2000). There are two types of osteoporosis, each with its own characteristics. Type I osteoporosis, also called postmenopausal osteoporosis, is characterized by an increase in bone turnover and an accelerated loss of trabecular bone, leading to vertebral fracture; it affects mainly postmenopausal women. Type II osteoporosis, also called senile osteoporosis, affects older women and men and is not accompanied by increased bone

turnover, but leads to hip fracture and has a greater mortality and morbidity than type I osteoporosis (Grynpas *et al.*, 2000).

Postmenopausal osteoporosis occurs when the arrest of ovarian function causes a natural depletion of estrogen in women and an increased rate of bone loss (Marx, 1980). Due to the larger surface area, bone loss is more apparent in trabecular bone, although some cortical bone loss also occurs. This increased rate continues for about 20 years, during which women lose 0.5 to 1.5 % of their peak bone mass every year (Marx, 1980). The rate of loss eventually decreases, but before it does a woman's bones may be significantly weakened.

Estrogen deficiency causes an increase in remodeling activity (increased osteoblastic and osteoclastic activity) (Eastell *et al.*, 1988). However, the resorption rate exceeds that of formation and over time there is net bone loss. Increased osteoclastic activity leads to deeper eroded cavities causing perforation in the trabeculae leading to a less connected trabecular network. Disconnectivity along with the decrease in trabecular bone volume cause a decrease in the structural integrity of the bone and leads to an increase in fracture risk (Parfitt, 1987).

1.2.1 The Aged Rat Model of Postmenopausal Osteoporosis

An animal model of postmenopausal osteoporosis can be defined as a living animal in which spontaneous or induced bone loss due to ovarian hormone deficiency can be studied, and in which the characteristics of the bone loss resemble those found in postmenopausal women (Kalu, 1991). Although in comparison to humans, the skeletal mass of rats remains stable for an extended period during their lifespan, rats can be ovariectomized to make them sex hormone deficient, and to stimulate the accelerated bone loss that occurs in postmenopausal women. Ovariectomy induced bone loss in the rat and postmenopausal bone loss share many similar characteristics. These include: increased rate of bone turnover with resorption exceeding

formation; an initial rapid phase of bone loss followed by a much slower phase; greater loss of trabecular bone than cortical bone; decreased intestinal absorption of calcium; some protection against bone loss by obesity; and similar skeletal response to therapy with estrogen, bisphosphonates, parathyroid hormone, calcitonin and exercise (Kalu, 1991). Furthermore, the aged rat (~ 9 months of age) has been determined to be a more suitable model than the young rat due to the concern that the rat model should be based on skeletally mature animals since human postmenopausal bone loss starts after the attainment of skeletal maturity. At nine months of age, the growth cartilage of the rat is closed and little to no osteogenesis is seen in the epiphyseal growth plate (Kalu *et al.*, 1989).

1.3 Bone Quality

Diagnosis of bone disorders has traditionally been achieved through evaluation of bone mineral density (BMD). In humans, measurement of BMD is a quick and non-invasive method of predicting fractures. However, extensive research over the past few decades has confirmed that it is insufficient to assess only bone density when predicting fracture risk (Van der Meulen *et al.*, 2001; Heaney, 1993; Jepsen *et al.*, 2003; Ott, 1993). For example, virtually every study that has contrasted mass density in patients with and without fragility fractures has found substantial overlap between the two populations (Melton *et al.*, 1989; Kimmel *et al.*, 1990). Thus, there is a need to evaluate overall bone quality, combining density with underlying material and structural properties. Relationships between overall bone fragility and the material and structural components of bone can be summarized in the following flowchart in Figure 1-3

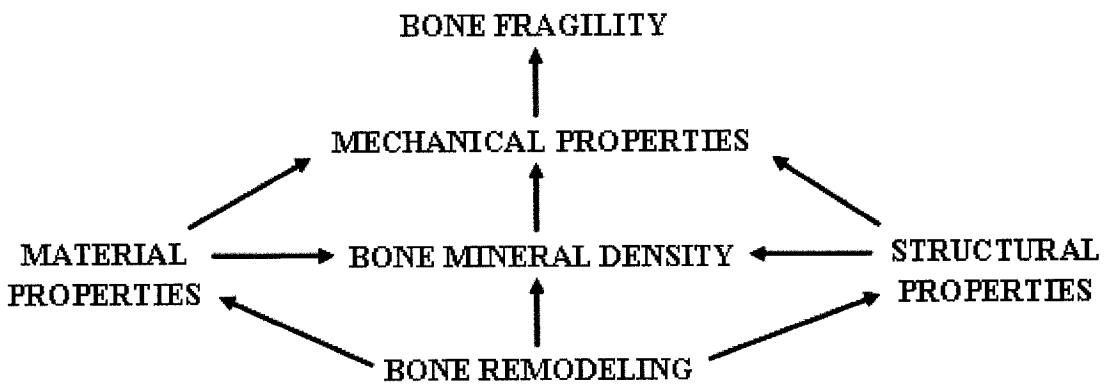

Figure 1-3: Relationship between bone fragility and various bone properties

As indicated in Figure 1-3, all of the underlying bone properties affect overall bone fragility either directly or indirectly. Therefore, bone fragility, which can be equated to the mechanical properties of bone, is dependent on material properties, which refer to the relative composition, quality and contribution of both phases of bone, and structural properties such as trabecular connectivity and its underlying architecture. Furthermore, both the material and structural properties are influenced by bone remodeling.

1.3.1 Bone Mineral Density

Bone mineral density (BMD) as measured by Dual Energy X-Ray Absorptiometry (DXA) is a measure of the amount of bone mineral density projected in a given area, not volume. Caution must notably be taken with this parameter, as areal BMD is not sensitive to density changes in all bone dimensions. Nevertheless, it is a quantitative technique that indicates the amount and density of bone and since it is non-invasive it is a useful and common clinical measure.

DXA is now the most common method of assessing BMD. DXA studies demonstrate that a decrease in BMD is correlated to the risk of fracture in osteoporotic women (Council of

the National Osteoporosis Foundation, 1996). Since many osteoporosis studies are performed in the rat, DXA has also been validated in rats as an accurate and precise technique to determine changes in BMD (Griffin *et al.*, 1993; Nagy *et al.*, 2001; Gala *et al.*, 1998; Sato *et al.*, 1994). Furthermore, measurements of excised lumbar vertebrae and femurs have shown to be a valid method to determine trabecular and cortical BMD (Sato *et al.*, 1994; Nagy *et al.*, 2001).

1.3.2 Mechanical Properties

Since mechanical properties are directly related to fracture risk, they are a much stronger predictor of mechanical integrity and propensity to failure than BMD measurements. However, mechanical testing is invasive and therefore can only be performed in animal models.

Because bone is anisotropic, it is vital to load bone in directions relevant to normal human loading. As such, several mechanical tests are performed on various bone sites to generate a broad overview of skeletal fragility. Typically, three-point bending tests are performed as a combined failure mode test, since the bone is tested both in tension and compression. Compression testing is typically performed on trabecular bone, due to simple sample preparation and set-up. Finally, torsion tests can be performed to test the shear behaviour of cortical bone. From these mechanical tests, the failure load, deformation, energy to failure and stiffness of bone are determined. Normalizing these data using the geometry of the bone provides information about the material properties including stress, strain, elastic modulus and toughness.

1.3.3 Material Properties

The composition of bone can be described in terms of the ratio of mineral to collagen phases. The contribution of the mineral phase to mechanical properties has traditionally held

more importance than the organic phase in the study of bone material characteristics (Burr, 2002). The quality of the mineral phase can be assessed using an overall distribution of mineralization and by testing the resistance to penetration.

Back scattered electron imaging is a method to obtain a mineralization profile. The bone surface is scanned in the scanning electron microscope and the electrons that are reflected directly from the sample, the back scattered electrons, are collected. Since the probability of a collision increases with increasing atomic number (number of protons in nucleus of atom), the intensity of detected electrons is related to the atomic number of the constituents. Since calcium has the heaviest nuclei, the intensity of detected electrons is related to calcium concentration and therefore, the degree of mineralization.

Microhardness provides a link between mineralization and material properties. To assess hardness, an indenter is pressed into a material and the relationship between load and size of indent reflects resistance to penetration and similarly hardness (Huja *et al.*, 2001). In this manner, microhardness is defined as the resistance to penetration. Microhardness has been shown to relate to mechanical properties; in particular to elastic modulus and yield strength (Evans *et al.*, 1990; Currey and Brear, 1990). Microhardness has also been shown to correlate to the degree of mineralization (Carlstrom, 1954). This is based on the fact that mineral is hard compared to its collagenous matrix. Therefore, a bone with a higher degree of mineralization will be more difficult to indent.

1.3.4 Structural Properties

Not only is the amount and quality of bone mass important in defining mechanical integrity, but fragility largely depends on how the bone is organized and arranged. Structural properties of cortical bone, specifically in shafts of long bones, include cortical thickness, cross-

sectional area and moment of inertia. Typically, the thicker and larger the cross-sectional area of a bone, the more load is required to fracture (Turner and Burr, 1993).

In terms of trabecular bone, structural properties are also highly influential in determining skeletal fragility. Structural properties refer to the overall microarchitecture of trabecular bone; the number, thickness and separation of individual trabeculae, as well as their relative connectivity. An increased number of thicker, less separated, and highly connected trabeculae are associated with higher failure loads (Mosekilde *et al.*, 1998; McCalden *et al.*, 1997). Disconnectivity or thinning and perforation of trabeculae weaken the trabecular network, which is evident in high turnover bone diseases such as osteoporosis.

Strut analysis is used to measure trabecular connectivity, which is determined from a 2-dimensional skeletonized image of a trabecular bone sample. Strut analysis determines connectivity by the amount of nodes (when a trabeculae connects with another trabeculae) and the number of free ends (a point where a trabeculae is not connected to another trabeculae) (Garrahan *et al.*, 1986). The loss of connectivity can be seen by a decrease in the number of nodes and an increase in the number of free ends (Compston *et al.*, 1993).

Women with postmenopausal osteoporosis have less connected trabecular bone, which is correlated with an increase in fracture risk. Ovariectomy of rats also causes the loss of connectivity, determined by strut analysis (Kinney *et al.*, 1998).

1.3.5 Bone Remodeling

Histomorphometry is a method of quantifying structural, formation and resorption parameters using Goldner's trichrome stained histological bone sections (Eriksen *et al.*, 1994). This stain allows the differentiation between mineralized bone and newly formed bone (osteoid). Formation is determined by measurement of osteoid volume, surface and thickness while

resorption is determined by directly measuring eroded surfaces of the trabeculae (Parfitt *et al.*, 1987). Analyzing formation and resorption parameters allows an overall assessment of remodeling. Estrogen deficiency in the OVX rat model causes a decrease in bone volume, an increase in bone formation and resorption as measured by histomorphometry (Lane *et al.*, 1999).

1.4 Growth Hormone

Human growth hormone (hGH), is a 22-kDa polypeptide synthesized in the pituitary and stored in the cells of the anterior pituitary (Kato *et al.*, 2002). In mature animals it is released from these cells in response to insulin-induced hypoglycaemia, starvation, amino acid infusion and by neural stimuli, including emotional stress (Orgu *et al.*, 2000). Two hypothalamic factors, growth hormone-releasing hormone (GHRH) and the inhibitory hormone somatostatin, interact to regulate GH secretion from pituitary somatotrophs. GHRH interacts with the pituitary GHRH receptors, and stimulates GH release from secretary granules as well as GH transcription (Kato *et al.*, 2002). Interaction of somatostatin with its receptors blocks GH release (Kato *et al.*, 2002). Once secreted, GH circulates bound to GH binding protein (GHBP), which is a soluble, extracellular domain of the GH receptor (GHR), and is generated from the GHR by proteolysis. The GHBP modulates GH action through a variety of mechanisms. It inhibits GH action thought antagonistic interaction with the GHR; that is, GHBP generates unproductive heterodimers with the GHR at the cell surface (Kato *et al.*, 2002). Furthermore, the GHBP prolongs the half-life of GH in the circulation by complexing with GH and delaying its elimination (Kato *et al.*, 2002). To mediate its biological effects, GH binds to the GHR.

GH influences various biological functions. The best-known property of GH is its ability to stimulate formation in the skeleton. GH levels increase significantly from childhood into adolescence, with peak GH levels corresponding to peak bone mass at approximately 20 years

of age (Monson *et al.*, 2002). From this point of peak bone mass, GH levels steadily decline throughout aging.

GH exerts many of its biological effects indirectly through the stimulation of insulin-like growth factor-I (IGF-I). Hepatocytes are well known to synthesize IGF-I upon GH stimulation and that systemically IGF-I is important in growth of bone and muscle. GH also has direct effects on many tissues including bone and the growth plate (Isgaard *et al.*, 1986).

Although GH is thought to be primarily involved in growth, it also influences the metabolism of major macromolecules including proteins, carbohydrates and lipid. Treatment with large doses of GH results in high blood glucose levels caused by the impairment of insulin sensitivity. GH stimulates amino acid uptake, protein synthesis and decreases protein oxidation (Butler and Le Roith, 2001). GH is also involved in the lipolytic pathway. Lipogenesis has been shown to be inhibited by GH and lipolysis stimulated (Butler and Le Roith, 2001).

Deregulation of GH secretion leads to many human diseases involving many organ systems. A deficiency of GH leads to dwarfism, increased obesity and low bone mass (Baroncelli *et al.*, 2003). An over expression of GH leads to gigantism and a bone disease called acromegaly (Kato *et al.*, 2002).

1.4.1 Growth Hormone Structure

The GH molecule is a globular protein consisting of four antiparallel α-helices (from residues 7-34, 75-87, 106-127 and 152-183), which are arranged in a left-twisted, tightly packed helical bundle. There are four cysteine residues within the GH molecule. The cysteine residues located at amino acids 57 and 165 form a disulphide bridge that creates a large loop at the N-terminal region of the molecule. In addition, a disulphide bond between Cys-182 and Cys-189 forms a small loop at the C-terminal end of the molecule (Ultsch *et al.*, 1994). These disulphide

bridges were conserved throughout evolution, suggesting their importance to the functioning of GH (Scanes and Campell, 1995).

The mechanism of GH-induced activation of the GH receptor has been studied extensively (Wells and de Vos, 1993). The hormone contains two receptor binding sites (Ultsch *et al.*, 1994). The first binding site consists of residues within helix 4 and to a lesser extent helix 1. The second binding site consists of residues within helix 3. Receptor activation involves dimerization in which a single GH molecule brings together two receptor molecules (Ultsch *et al.*, 1994). Signal transduction via the JAK/STAT pathway follows.

1.4.2 Effect of Growth Hormone on Adiposity

The metabolic effects of GH on adipose *in vivo* are variable and complex, apparently consisting of at least two components; an early insulin-like effect followed by a later more profound anti-insulin effect (Natera *et al.*, 1994). The results of the latter effect may include both a stimulation of lipolysis and an inhibition of lipogenesis. The anti-lipogenic effect of hGH has been substantiated with the demonstrations of the decrease of the expression of glucose transporter 4 (GLUT4) in adipocytes (Tai *et al.*, 1990), the inhibition of the activity of acetyl-CoA carboxylase in adipose tissues (Ng *et al.*, 2000), and the reduction of glucose incorporation into isolated cells and tissues (Ng *et al.*, 1990).

1.4.3 Skeletal Effects of Growth Hormone

It has long been known that excess GH clearly affects the structure and dynamics of bones of patients with acromegaly (Bouillon, 1991; Inzycchi and Robbins, 1994). The most striking clinical features of acromegaly are due to the excessive growth of bone after closure of the epiphyseal growth plates. Total bone BMD is frequently increased in acromegaly with a

greater increase in cortical bone than in trabecular bone (Bouillon, 1991; Inzycchi and Robbins, 1994). In contrast to patients with acromegaly, adults with childhood-onset GH deficiency exhibited decreased bone mass and increased fracture incidence compared to age-matched controls (Saggese *et al.*, 1993). Based on the finding that bone mass is increased in acromegaly and decreased in GH deficiency, it has been postulated that GH promotes bone formation to a greater extent than bone resorption at each remodeling site and, thus, results in positive bone balance.

Almost four decades ago, Harris and Heany (1969) clearly demonstrated that GH administered to adult dogs led to a marked increase in bone mass. Isaksson and co-workers have demonstrated that the unilateral administration of GH into the tibial epiphyseal growth plate of hypophysectomized rats stimulated bone growth on the injected side only (Isaksson *et al.*, 1987). Subsequently, Baker *et al.* (1992) have shown that osteoblast-specific overexpression of GH in transgenic mice is able to stimulate bone growth directly without significant systemic effects . Consistent with these data, several *in vitro* and *in vivo* studies have demonstrated that GH is important in the regulation of bone formation (Canalis, 1995; Clark, 1997; Marcus, 1997).

According to the original somatomedin hypothesis, GH has been proposed to stimulate skeletal growth indirectly by stimulating liver production of IGF-I to act in an endocrine manner to stimulate bone growth (Daughaday and Rotwein, 1989). Subsequent studies, however, have shown that GH has direct action on bone (Ernst and Rodan, 1990; Schmid *et al.*, 1994; Ernst and Froesch, 1988; Mohan *et al.*, 1992). Based on the finding that osteoblasts contain GH receptors (Nilsson *et al.*, 1995) and that GH treatment increases the production of IGF-I in rat osteoblast-

like cells (Ernst and Froesch, 1988), it has been proposed that GH may exert its direct effects via GH receptors to stimulate the local production of IGF-I to act in an autocrine/paracrine manner.

1.4.4 Effect of Growth Hormone on the Rat Skeleton

The effects of hGH on the rat skeleton have been extensively studied. GH causes an increase in cortical bone formation of both young and old rats as shown through increases in BMD and cortical bone thickness. (Andreassen *et al.*, 1996; Jorgesen *et al.*, 1991). Mechanical testing of the femur by three-point bending resulted in increased ultimate load and moment of inertia but did not have an effect on stress or elastic modulus (Mosekilde *et al.*, 1999).

Studies indicate that GH increases cortical bone mass in aged rats as well as in aged OVX rats (Verhaeghe *et al.*, 1996; Wang *et al.*, 2001). Administration of GH to aged OVX rats increased femoral load values but did not increase stress or elastic modulus values (Andreassen and Oxlund, 2000; Mosekilde *et al.*, 1998). Furthermore, the significant increases in femoral strength were only seen at GH doses greater than 2 mg/kg/day (Mosekilde *et al.*, 1998).

Histomorphometric studies have shown a limited effect of GH on trabecular bone. Gunness and Hock demonstrated that GH treatment in intact 18 month-old rats resulted in no significant increase in trabecular bone volume, mineralizing surface, mineral apposition rate or bone formation rate (Gunness and Hock, 1995). Furthermore, in younger sham rats treated with GH no significant increases were observed in vertebral or femoral neck strength (Andreassen *et al.*, 1996).

1.4.5 Growth Hormone Peptides

Human growth hormone is responsible for biological actions that include the reduction and redistribution of body fat, the regulation of lipid metabolism and the promotion of growth

(Ogru *et al.*, 2000). Since hGH exerts multiple biological actions in the body, there may be more than one mechanism by which GH mediates its response. One idea that has been raised is that GH may act as a prohormone that would require proteolytic processing in peripheral tissues to exert its full range of biological activity (Garcia-Barros *et al.*, 2000). The idea is supported by the discovery of active peptides and isoforms circulating in the human blood stream (Sinha and Jacobsen, 1994).

Advances in peptide synthesis have made it possible to produce specific and discrete functional domains of hGH. For example, the insulin-like actions of hGH reside in the amino-terminal region of the molecule [hGH-(6-13)] (Heffernan *et al.*, 2000). Furthermore, the carboxy terminus of the hGH molecule [hGH-(177-191)] has been identified as the lipid mobilizing domain of the intact hormone (Heffernan *et al.*, 2000). This peptide has been shown to have similar action on adipose tissue as the intact hGH and has been suggested to be the lipolytic domain of the hGH molecule.

1.5 Anti-Obesity Drug (AOD) 9604

Due to the lipid metabolizing effects of the C-terminal domain of hGH residues (hGH177-191), combined with the lack of diabetogenic effect (Heffernan *et al.*, 2001b), this peptide is currently being considered as a potential anti-obesity drug (AOD). AOD is a 15-residue, disulfide-bonded cyclic peptide, cyclo(6,13)-H_2N-Leu-Arg-Ile-Val-Gln-Cys-Arg-Ser-Val-Glu-Gly-Ser-Cus-Gly-Phe-OH (Ogru *et al.*, 2000). With the addition of tyrosine for stability, AOD is called AOD9604, which is the peptide currently under investigation. X-ray crystal structure analysis of intact, native hGH shows that the C-terminal domain of hGH has a disulfide bond between residues 182 and 189 and that residues 177-182 form part of an α-helix (Orgu *et al.*, 2000). Structurally, AOD is similar to the intact hormone (Orgu *et al.*, 2000).

1.5.1 Effect of AOD on Adiposity

Several studies have been performed to compare AOD and hGH actions on lipid metabolism. Physiologically, they appear to have the same effect. AOD has been shown to decrease the body weight in an obese mouse (Heffernan *et al.*, 2001b). Furthermore, AOD reduces lipogenic activity (Orgu *et al.*, 2000; Heffernan *et al.*, 2000; Wu and Ng, 1993) and increases lipolytic activity and fat-oxidation (Ogru *et al.*, 2000; Heffernan *et al.*, 2000; Heffernan *et al.*, 2001b). However, while the effects of AOD and hGH appear to be similar, the time required to achieve them differs. The lipolytic effect of AOD was seen in minutes as opposed to the four hours that it took in hGH (Ogru *et al.*, 2000; Wijaya and Ng, 1993). This discrepancy was interpreted as the time required for post-translational activation of the hormone and the release of bioactive domains form the molecule to act on target tissues (Wijaya and Ng, 1993).

In addition to a change in rate of effect, the mechanisms also appear to differ. Although the binding site of AOD is unknown, it has clearly been shown in competition studies that it is not the GHR (Ogru *et al.*, 2000; Heffernan *et al.*, 2001c; Ng *et al.*, 2000). Nonetheless, AOD appears to have the same downstream actions as hGH on lipid metabolism although it is mediated differently (Heffernan *et al.*, 2000).

Metabolic studies show that AOD upregulates β_3-adrenergic receptor (β_3-AR), a lipolytic receptor found extensively in rat adipose cells, which initiates the lipolytic cascade (Heffernan *et al.*, 2001c). Normally the pathway of β_3-AR upregulation is due to the binding of GH but AOD does not directly bind. Therefore, there may be an indirect mechanism that caused the increased β_3-AR. As well, AOD has been shown to inhibit acetyl-CoA carboxylase, a key catalyst in the lipogenesis pathway (Wijaya and Ng, 1993).

1.5.2 Skeletal Effects of AOD

Since postmenopausal osteoporosis is characterized by bone resorption that exceeds bone formation, antiresorptive agents can help to restore skeletal balance by reducing bone turnover, primarily at the tissue level. This applies to bisphosphonates, including cyclically administered etidronate, or the preferred compounds alendronate and risedronate; to selective estrogen receptor modulators (SERMs), most notably raloxifene; and to calcium-vitamin D supplements (Meunier, 2001). All these treatments reduce bone turnover by inhibiting osteoclast activity. However, all these treatments have the same limitations: bone mass is not restored, the fracture risk is still 50% or greater, and the increase in BMD is moderate and primarily ascribable to an increase in mean bone tissue mineralization rather than an increase in bone tissue (Boivin *et al.*, 2000).

Another therapeutic approach is anabolic – namely, to enhance bone formation. Anabolic agents differ fundamentally from antiresorptive drugs in their primary mechanism of action; that is, they directly stimulate bone formation. The potential of anabolic agents to improve bone density more substantially than antiresorptives suggests that they might reduce fracture risk to a greater extent. These bone formation stimulators include GH, IGF-I, and parathyroid hormone (PTH).

The rationale for considering GH as a potential anabolic agent is that it is critical for the acquisition and maintenance of bone mass. Since GH stimulates bone formation in the skeleton (i.e. anabolic effect) it is important to understand if this skeletal effect is conserved in AOD. Previously, AOD was shown to be mitogenic in primary osteoblast cultures and to have no effect on the activity of mature osteoclasts (Cornish, 2002). Therefore, it appears that AOD has the profile of a bone anabolic and may have potential as a therapeutic compound in the bone

area. More recently, we have shown AOD to prevent ovariectomy-induced fragility and bone loss in an aged rat model of postmenopausal osteoporosis (Rowe, 2007). This was a preventative rather than a treatment study due to the fact that AOD administration was initiated immediately after the rats were ovariectomized. AOD's effects appeared to be dose dependent, with a dose of 0.25 mg/kg/day having the most protective capacity, and site-specific, with cortical effects more pronounced than trabecular effects (Rowe, 2007). Furthermore, a dose study looking at the skeletal effects of 0.001, 0.003, 0.01, 0.03, 0.1 and 0.3 mg of AOD/kg/day on 3 month-old ovariectomized rats revealed that AOD has maximum protective effects against OVX –induced fragility at doses of 0.01 and 0.25 mg/kg/day (unpublished data).

1.6 Hypothesis and Objectives

In this study, we are testing the overall hypothesis that AOD9604 will rebuild the bone lost during ovariectomy (OVX) in a rat model of postmenopausal osteoporosis.

The specific objectives of the study are:

i. To determine if treatment with AOD9604 after OVX can rebuild bone mass.

ii. To determine if AOD9604 treatment after OVX can restore bone structure and decrease bone remodelling.

iii. To establish whether AOD9604 treatment reverses the effects of OVX on bone mechanical properties.

iv. To determine the effects of AOD9604 treatment on bone mineralization.

Chapter 2 : Methodology

2 Introduction

The following chapter outlines the experimental set-up and various techniques used to evaluate bone quality. A brief technical background is also presented, along with the identification of the important parameters derived from each test.

2.1 Animal Care and Housing

This study included a total of 75 female Sprague-Dawley rats (*Rattus Norvegicus*), approximately nine months of age (retired breeders), purchased from Harlan (Harlan Farms, Indiana). These rats were housed at the animal facility of the Division of Comparative Medicine at the University of Toronto (Toronto, Ontario). After a 1-week acclimatization period, the veterinarians removed the ovaries (ovariectomy, OVX) of 60 rats. All operations were performed on the same day. The rats were then given identification ear-clips and transferred into transparent plastic cages for the remainder of the study. The cages were lined with cornmeal bedding and contained a hide-away tube as well as an unlimited supply of tap water and lab chow. All of these cages were in the same room, which was monitored daily for temperature and humidity and the lights were set on a 12-hour on/off cycle. Furthermore, the rats were monitored throughout the entire study for any signs of illness or stress.

2.2 Drug Preparation and Administration

Three separate drug doses were used: 0.01 mg/kg/day, 0.03 mg/kg/day, and 0.25 mg/kg/day. These weight-based dosages were achieved by weighing the rats every week and adjusting concentrations accordingly. The drug was reconstituted daily by weighing

the peptide powder and adding distilled water to achieve the calculated concentration. When the powder fully dissolved it was injected into sterile vials using a syringe.

The vials were brought to the veterinary technicians at the Division of Comparative Medicine at the University of Toronto (Toronto, Ontario) who administered the solution by gavages. Doses were given 5 days a week over a 12-week period. All rats were rewarded daily with a fruit loop.

2.3 Experimental Design

2.3.1 Treatment Groups

This recovery study was designed to test three different doses of AOD (0.01, 0.03, 0.25 mg/kg/day) in OVX skeletons. To achieve this, the 75 rats were divided into 5 groups of 15 as shown in Table 2-1.

Table 2-1: Treatment groups and AOD dosages

Model	Group	Abbreviation	Number of Rats	Dose (mg/kg/day)
Normal	Control	NC	15	0
OVX	Control	OC	15	0
OVX	AOD-0.01	O(0.01)	15	0.01
OVX	AOD-0.03	O(0.03)	15	0.03
OVX	AOD-0.25	O(0.25)	15	0.25

2.3.2 Experimental Timeline

The study was timed to provide a 12-week period of OVX-induced bone loss, and a 12-week dosing period for treatment groups and weight-based AOD concentrations as shown in Figure 2-1.

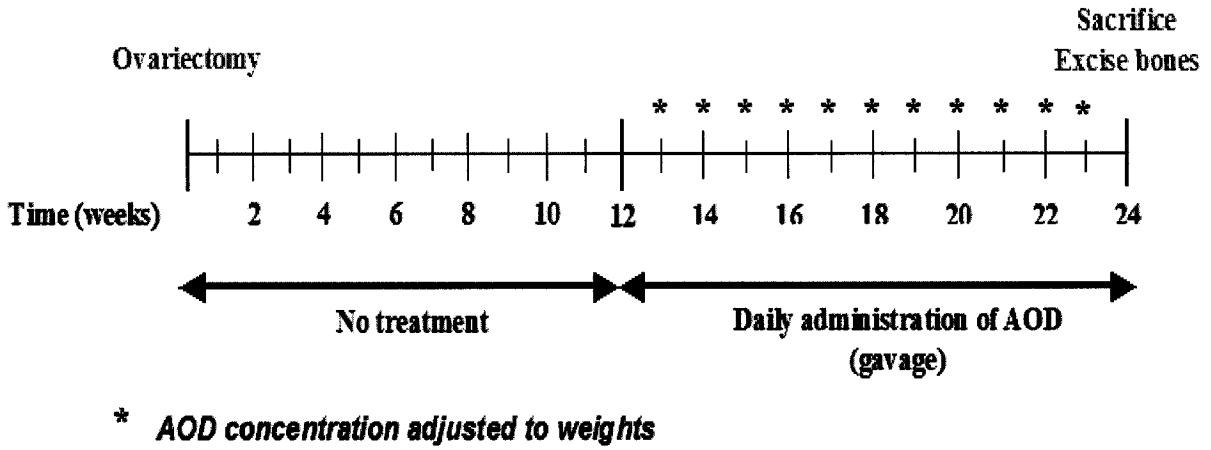

Figure 2-1: Experimental Timeline

2.3.3 Sacrifice and Dissection

Following the 12-week treatment period, each rat was euthanized via exsanguination in a CO_2 chamber followed by cervical dislocation. The control groups were sacrificed exactly at the 12-week point and the treatment groups were sacrificed one day later due to time constraints.

Immediately after sacrifice, the spines along with the femurs and tibia of each rat were roughly excised and inserted into pre-labelled plastic tubes for further processing. These tubes were then placed onto a bed of ice after which they were transferred to a freezer and maintained at (-20°C). The right tibiae were dissected and fixed in 70% ethanol for histomorphometry.

2.3.4 Experimental Techniques

The experimental techniques performed are summarized in Figure 2-2. Unless otherwise indicated, all samples were handled in the same manner and evaluated using all the techniques.

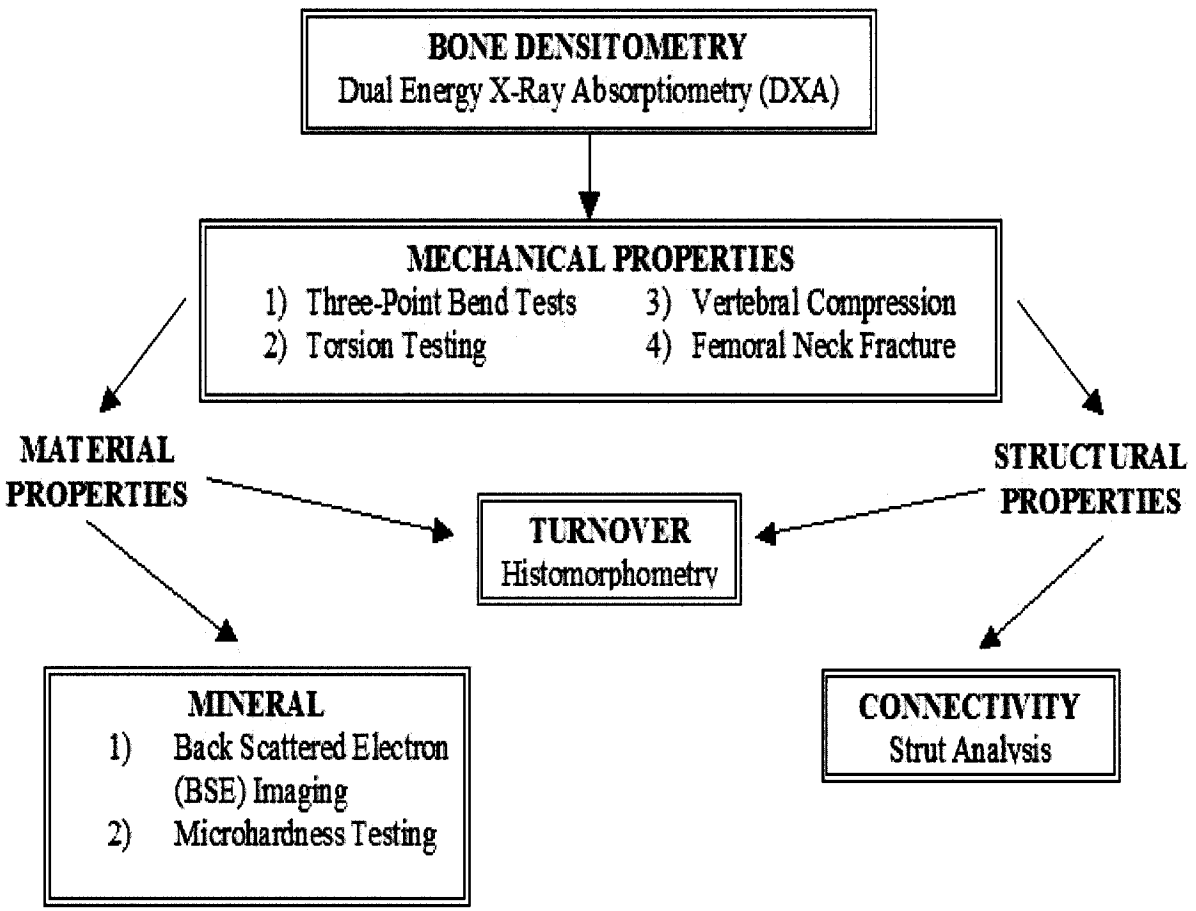

Figure 2-2: Flowchart of experimental techniques used to assess bone quality

2.4 Bone Densitometry

Dual Energy X-ray Absorptiometry (DXA), using a PIXImus™ densitometer (Lunar GE Corporation), was used to determine bone mineral content (BMC) and areal bone mineral density (BMD). The DXA technique employs a cone beam x-ray source that generates two energies: 35 (low) and 80 (high) keV. As photons transverse the tissue, they are either absorbed or scattered, depending on their attenuation properties. The detector assumes that the object being scanned consists of 3 components that can be distinguished by their x-ray attenuation properties: bone mineral, fat, and lean soft tissue. To distinguish bone mineral, a threshold value is calibrated and set by the PIXImus™ to distinguish between pixels that are considered bone and those that are soft tissue alone (Pietrobelli *et al.*, 1996). The amount of bone mineral content (g) is then divided by the projected bone area (cm^2) to give an areal bone mineral density (g/cm^2) measurement.

The PIXImus™ was calibrated with an aluminum/lucite phantom prior to each scanning session. Tests were performed on the left femurs and lumbar vertebrae (4-6). The excised and cleaned left femurs and lumbar vertebrae (4-6) were removed from the freezer and kept on a bed of ice prior to testing. Bones were placed in the desired configuration on a polystyrene plate that simulates soft tissue thickness on bone. Femurs were placed individually on the plate caudal side down and vertebrae were also placed caudal side down but in a row of three to simulate the natural arrangement in the skeleton (see Figure 2-3).

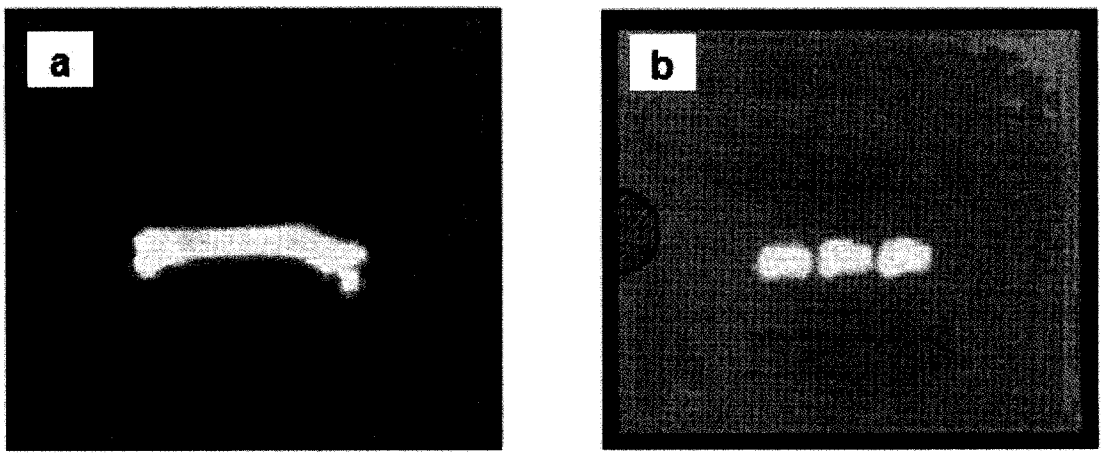

Figure 2-3: DXA scan of the projected area of the (a) femur and (b) vertebra

2.5 Evaluation of Bone Mechanical Properties

Destructive mechanical testing of whole bone is an effective way to determine overall skeletal fragility. There are several biomechanical parameters that can be used to describe the mechanical fragility or integrity of the bone. The basic relationship is that between the amount of load required to fracture the bone and the resulting displacement or deformation of the specimen. A load-displacement curve is generated for every sample tested (see Figure 2-4a). The slope of the linear region of this curve is termed the extrinsic stiffness (S; N/m) or rigidity of the specimen. This linear region represents elastic behaviour, meaning that the specimen will return to its original shape if a load is applied and removed within this region. The transition from the elastic region to plastic region is noted by the yield point. Ultimate load (F_u; N) represents the maximum force applied to the specimen, while failure load (F_f; N) represents the force at which the specimen actually failed or fractured. Most often, the ultimate and failure loads are equivalent for a given bone specimen. The failure displacement (d_f; mm) represents the maximum deformation achieved prior to fracture, and is related to the ductility of the specimen. Finally, the area under the load-displacement curve up to the point of failure is termed the energy to failure (U_f; mJ), and represents the amount of energy required to cause failure. Because each of these parameters defines a different mechanical property, it is important to take note of all the parameters to generate a comprehensive view of mechanical integrity.

To eliminate effects caused by geometric or size-dependent differences between specimens, it is necessary to normalize the load-displacement curve. This is achieved by using standard engineering formulae, which convert the load-displacement curve into a

stress-strain curve (see Figure 2-4b). It is important to note however, that these formulae assume that the specimen is homogeneous in shape/area and composition along its length (Van der Meulen *et al.*, 2001). Since bone is a composite material of several hierarchical levels and its shape/area changes along its length, normalization using engineering formula represents only an approximation of the true stress/strain behaviour. Nonetheless, following normalization of the load-displacement curve, the ultimate and failure force are represented by the ultimate (σ_u; MPa) and failure stress (σ_f; MPa), respectively. Failure displacement is represented by failure percent strain (ε; %). The slope of the linear region is termed the elastic or Young's modulus (E; MPa), and is a measure of the intrinsic stiffness of the material. The yield point is defined as the intersection point between the stress-strain curve and a line drawn parallel to the linear portion of the stress-strain curve and offset by 0.2% strain (Turner and Burr, 1993). Finally, the area under the stress-strain curve is termed toughness (U_f; J/mm^3), which also represents the amount of energy required to cause failure per unit volume of bone.

The anisotropic nature of bone, as well as the contribution of both cortical and trabecular components in any given bone, necessitates the use of several different mechanical tests. Three-point bending tests long bones in both tension and compression at a pre-determined position (midpoint). This test is typically done on femora, and is representative of cortical bone mechanical properties. Sample preparation and setup are fairly routine in this test, which increases its repeatability and accuracy. Torsion testing represents a mechanical test that evaluates the shear behaviour of cortical bone. This is typically done on femora as well, and is designed so that failure occurs at the weakest point along the cortical bone shaft. Compression testing is typically done on individual

vertebrae due to the small physical size of the sample and minimal sample preparation. Since compressive fractures are often seen in osteoporotic bone, this test can be considered to be clinically relevant (Marx, 1980). While both cortical and trabecular bone are present in individual vertebra, vertebral compression is generally accepted as a test for trabecular bone mechanical properties (Turner and Burr, 1993). Finally, a type of cantilever testing is performed on the proximal end of femora to evaluate the mechanical integrity at the clinically relevant femoral neck. Similar to the vertebrae, the femoral neck represents a site that is especially sensitive to skeletal fragility (Jamsa *et al.*, 1999). Femoral neck fracture is representative of a combined model of both cortical and trabecular bone. All four mechanical tests were performed on the excised bones of all sample groups.

(a)

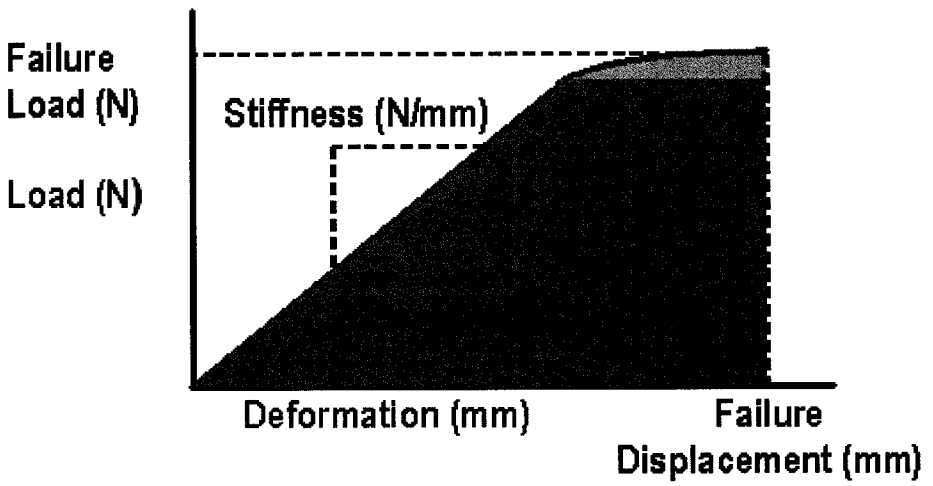

(b)

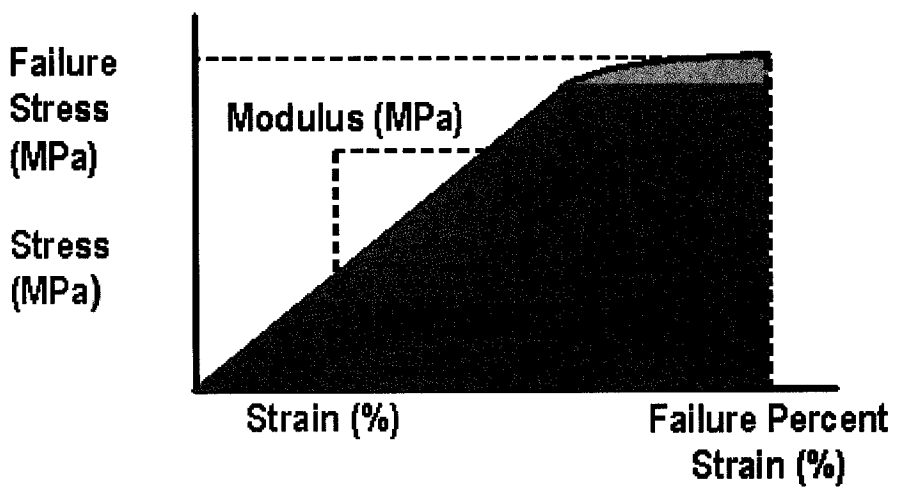

Figure 2-4: (a) Idealized load-displacement curve and (b) idealized stress-strain curve

2.5.1 Three-Point Bending

The right femur was used for the three-point bending test. Samples were allowed to thaw to room temperature in saline-wrapped gauze prior to testing. During this transition period, the bones were measured to determine the placement of the sample on the jig. First, the length of the bone was measured with digital callipers. From the distal end of the femur, a mark was placed on the bone at 25% of the entire length. From this point, a second mark was placed at 15.6 mm, the set gauge length, and finally a mark was placed the midpoint of the gauge length (Turner and Burr, 2001).

Testing was completed on a mechanical testing machine (Instron 4465, Instron Canada Inc.) using a 1000 N load cell. The load cell was calibrated and balanced after the three-point bending jig was installed. The stainless steel jig, used for testing, consisted of a base with two supports and an indentor that was attached to the crosshead of the Instron.

All samples were placed in the same orientation, with the anterior side facing upwards, resting naturally on the supports in their most stable position. The gauge length marks were aligned with the 2 supports of the jig and the indentor was aligned with the midpoint of the gauge length as shown in Figure 2-5.

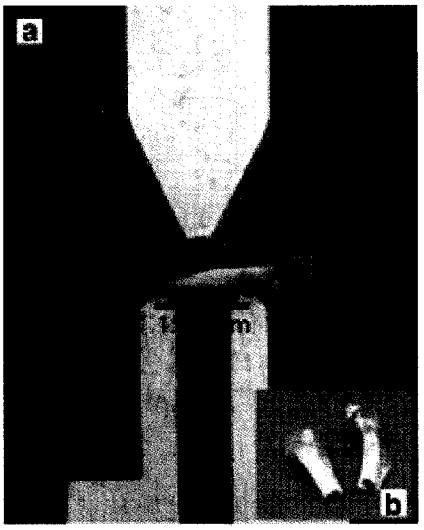

Figure 2-5: Three-Point Bending a) bone placement in appartus b) bending fracture

The bones were preloaded to approximately 1.0 N. The test was run at a speed of 1 mm/min until failure. Load versus time data was acquired from the Instron every 0.1 seconds by LabView data acquisition software (National Instruments Corp.; Austin, TX). Displacement was then determined given the test speed and the time data points. A load-displacement curve was created for every sample, and from this curve failure load, stiffness, failure displacement and energy to failure were determined. Figure 2-6 displays a typical load-displacement curve generated from the three-point bending test. The failure point was consistently chosen as the point where load is significantly reduced and identified as a sharp vertical drop.

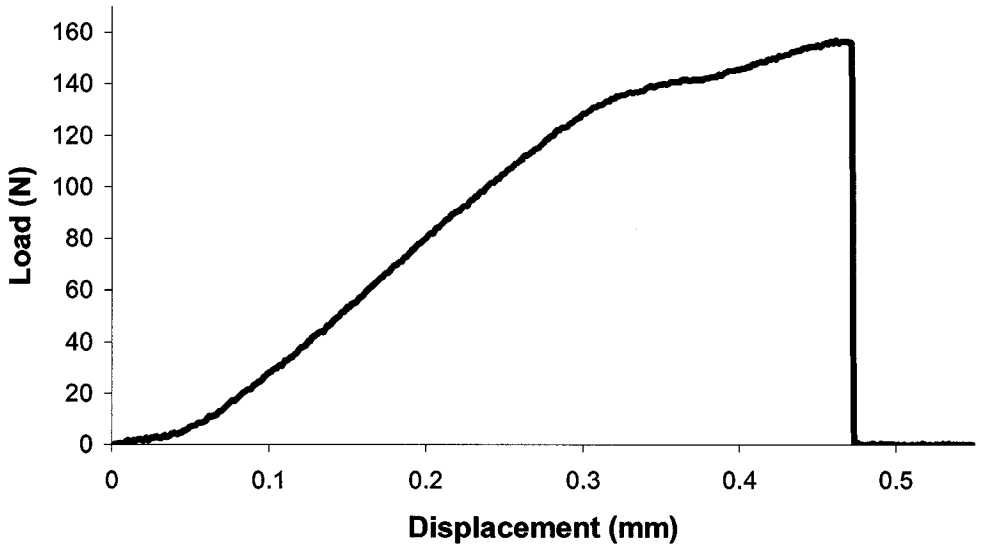

Figure 2-6: Typical load-displacement curve generated from three-point bending test

To eliminate differences caused by geometrical variation, load-displacement data was normalized by femoral transverse sections. Upon failure, the distal end of the fractured femur was pressed into Fimo (Fimo Classic, Eberhard Faber) such that the fracture surface faced upwards. The Fimo and femur combination was then placed in an embedding mold along with an ID tag (see Figure 2-7b). Epoxy was poured into this mould and left to harden for 48 hours. The hardened blocks were sliced, using a low speed saw (Isomet, Bueler), as close to the fracture surface as was possible while still maintaining the full cross-section of the bone (see Figure 2-7c). The epoxy embedded blocks were secured onto a plexiglass plate using Fimo. Images of the femoral cross-section were obtained using a scanning electron microscope (solid state BSE detector, FEI Company, Hillsboro, OR, USA; FEI XL300ESEM). Beam conditions were set at 20

kV accelerating voltage, 78 μA current, and magnification 100x. To eliminate charge effects, the images were obtained while the scanning electron microscope (SEM) was in variable pressure mode. External anterior-posterior and medial-lateral diameters (mm), cross-sectional area (mm^2), cortical thickness (mm), and moment of inertia (mm^4) were then measured from these binarized images using image analysis software (ImageJ 1.28u, National Institute of Health; see Figure 2-8).

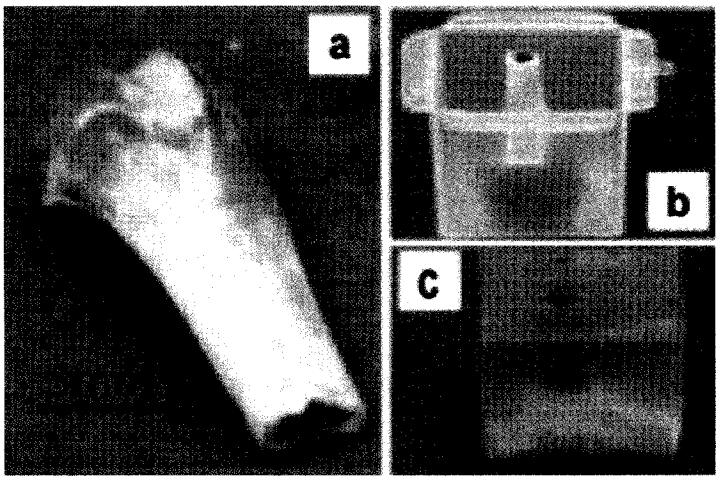

Figure 2-7: Embedding the distal end of the right femur in epoxy

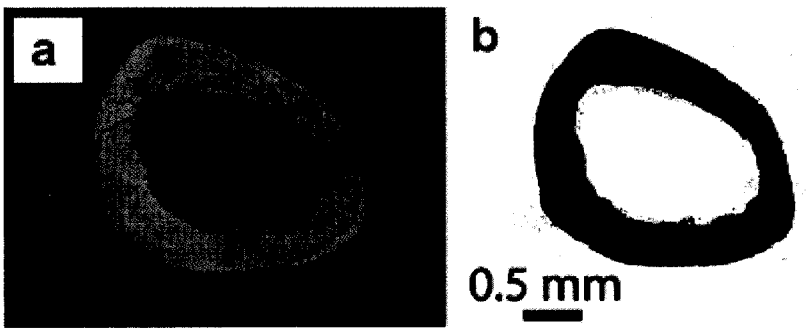

Figure 2-8: SEM image of femur cross-section (a) and binarized image of femur cross-section (b)

Stress-strain curves were created from the normalized data. Normalized material properties taken from the stress-strain curve included failure stress, failure strain, elastic modulus, and toughness which were determined by the formulae listed below (Turner and Burr, 2001):

$$\sigma_f = \frac{F_f l_o \phi_{AP}}{8 I_{xx}}$$

σ_f : *Failure stress* (*MPa*)
F_f : *Measured failure load* (*N*) [Equation 1]
l_o : *Gauge length* (*mm*)
ϕ_{AP} : *External diameter in anterior – posterior direction* (*mm*)
I_{xx} : *Elliptical moment of inertia* (mm^4)

$$\varepsilon_f = \frac{6 \phi_{AP} \delta_f}{l_o^2} \cdot 100$$

ε_f : *Failure strain* (%) [Equation 2]
ϕ_{AP} : *External diameter in anterior – posterior direction* (*mm*)
δ_f : *Failure displacement* (*mm*)
l_o : *Gauge length* (*mm*)

$$E = \frac{K l_o^3}{48 I}$$

E : *Elastic* mod*ulus* (*MPa*) [Equation 3]
K : *Stiffness* (*slope of load – deformation curve*) (N/mm)
l_o : *Gauge length* (*mm*)
I : *Elliptical moment of inertia* (mm^4)

$$\mu_f = \sum_{j=1}^{n} (\sigma_{j-1})(\varepsilon_{j-1} - \varepsilon_j) + \left[\frac{(\sigma_{j-1} - \sigma_j)(\sigma_{j-1} - \sigma_j)}{2} \right]$$

μ_f : *Toughness* (mJ / mm^3)

σ : *Stress* (MPa) [Equation 4]

ε : *Strain*

n : *Total number of data points to yield*

j : *Integer increments from* 1 *to* n

2.5.2 Torsion Testing

The excised left femora of all rats were tested to failure in torsion to evaluate the mechanical properties of cortical bone in a different mode. Torsion testing allows us to apply shear loads to the bone so that it fails at its weakest point, rather than forcing it to fail at a predetermined midpoint, as is the case for the three-point bending test (Brodt *et al.*, 1999). Similar to three-point bending, femora were allowed to thaw to room temperature in saline-wrapped gauze, the average length (mm) per femur was determined using digital callipers, and the midpoint marked with a waterproof marker. The extremities of the femur were removed using a low speed saw (Isomet, Bueler). A 16 mm gauge length was then marked on the severed bone and a 16 mm strip of saline soaked gauze was wrapped around the gauge length (see Figure 2-9a). The gauze remained on the bone until testing and was kept moist with saline at all times.

The bone was then secured within two bolt heads using a customized jig. To achieve this, the wrapped bone was first placed vertically into a bolt head and secured with polymethylmethacrylate (PMMA) (see Figure 2-9b). The PMMA was allowed 10 minutes to dry before the bone-bolt assembly was inverted (see Figure 2-9c). Beneath this inverted assembly, a second bolt was placed and nuts were used to fix it at the required height position. The lower bolt head was filled with PMMA and the inverted bolt-bone assembly was screwed down so that the remaining free end was secured in PMMA (see Figure 2.9d). The PMMA was allowed 10 minutes to dry before the bolt-bone-bolt assembly was removed from the jig.

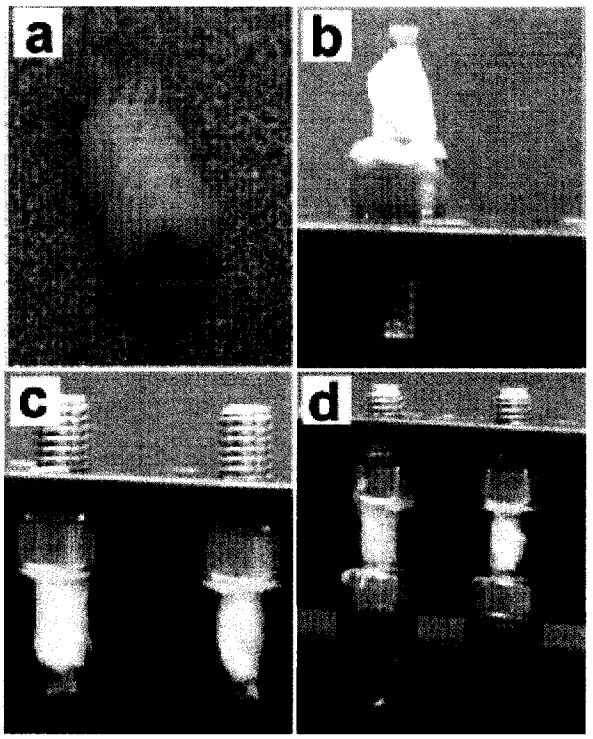

Figure 2-9: Bone preparation for torsion testing a) gauze wrapped bone b) bone placement in bolt c) inverted bolts d) bolt-bone-bolt assembly

Torsion testing was performed on a calibrated custom-design torsion device, which consisted of one stationary and one rotating chuck along with a 20in·lb load cell and a gauge to measure the angle of rotation. The load cell was verified and speed of rotation measured before testing.

The bolt-bone-bolt assembly was carefully secured into the chucks as shown in Figure 2-10. The gauze was removed immediately before testing. Tests were run at approximately 0.7 radians/minute until failure, and data were collected every 0.1 seconds by LabView data acquisition software (National Instruments Corp.; Austin, TX). From the collected data, a torque-angular displacement curve was created, as illustrated in Figure 2-11. Unnormalized mechanical properties were determined from the torque-

angular displacement curve including failure torque, angular deformation at failure, energy to failure and stiffness.

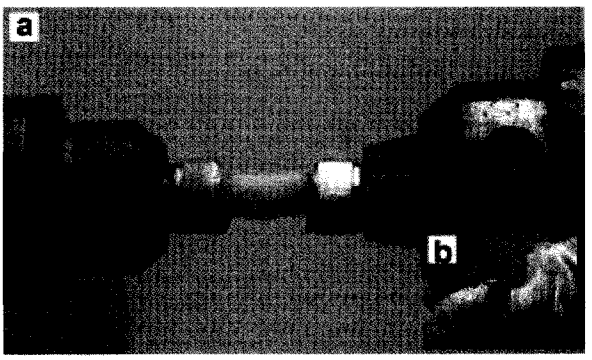

Figure 2-10: Torsion testing a) bone placement in apparatus b) torsion fracture

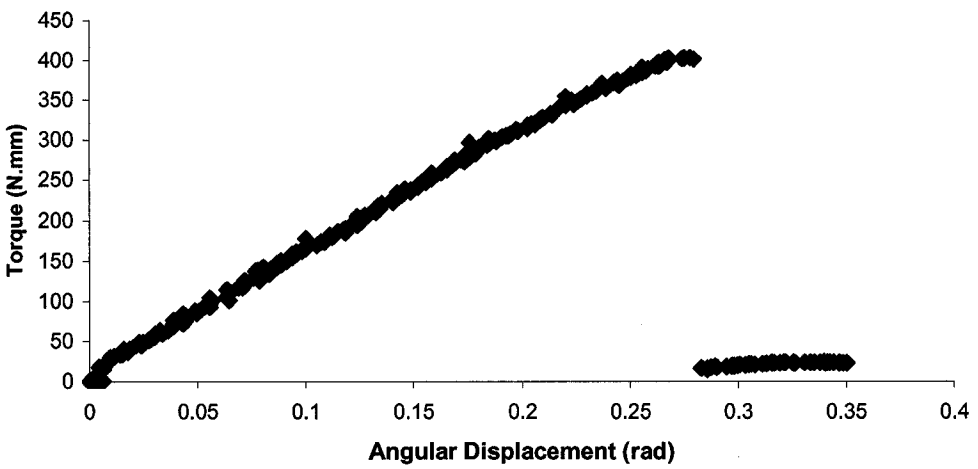

Figure 2-11: Typical torque-angular displacement curve generated from torsion testing

To eliminate differences caused by geometrical variation, torque-angular displacement data were normalized by the same transversal sections of the contralateral (right) femora (embedded in epoxy blocks following three-point bending). It was

impossible to normalize these tests with geometrical data from the left femora, as torsion testing results in destructive spiral fractures along the length of the bone. Moreover, it has been previously shown that geometrical properties do not significantly differ between the left and right femora within the same animal (Battraw *et al.*, 1996). The major external diameter (medial-lateral direction) and the polar moment of inertia (J; mm^4) were determined and used to convert the torque-angular displacement curve into a stress-strain curve. Normalized material properties taken from the stress-strain curve include failure shear stress, shear strain at failure, toughness and shear modulus. The formulae used to calculate the normalized properties are as follows (Turner and Burr, 2001):

$$\sigma_f = \frac{\phi_{ML}}{2} \cdot \frac{T_f}{J}$$

σ_f : *Failure shear stress* (MPa) [Equation 5]
T_f : *Failure torque* $(N \cdot mm)$
ϕ_{ML} : *External diameter in medial – lateral (major) direction* (mm)
J : *Polar moment of inertia* (mm^4)

$$\varepsilon_f = \frac{\phi_{ML}}{2} \cdot \frac{\alpha_f}{l_o} \cdot 100$$

γ_f : *Failure shear strain* (%) [Equation 6]
ϕ_{ML} : *External diameter in medial – lateral (major) direction* (mm)
α_f : *Failure rotation* (mm)
l_o : *Gauge length* (mm)

$$G = \frac{sl_o}{J}$$

G : *Shear modulus (GPa)*

s : *Stiffness* $(N \cdot mm / rad)$ *or* (mJ / rad) [Equation 7]

l_o : *Gauge length* (mm)

J : *Polar moment of inertia* (mm^4)

$$\mu_f = \sum_{j=1}^{n} (\sigma_{j-1})(\varepsilon_{j-1} - \varepsilon_j) + \left[\frac{(\sigma_{j-1} - \sigma_j)(\sigma_{j-1} - \sigma_j)}{2} \right]$$

μ_f : *Toughness* (mJ / mm^3)

σ : *Stress* (MPa) [Equation 8]

ε : *Strain*

n : *Total number of data points to yield*

j : *Integer increments from* 1 *to* n

2.5.3 Vertebral Compression

The 6th lumbar vertebra (L6) was used for compression testing. The vertebrae were trimmed of all processes, leaving only the vertebral body for testing. The samples were removed from the freezer at least two hours before testing to ensure the bones were completely defrosted. The vertebrae were individually wrapped in saline soaked gauze during defrosting.

Coronal and transversal images of the individual vertebrae were obtained using a macroscope connected to a digital camera (see Figure 2-12). Images were then analyzed using image analysis software (ImageJ 1.28u, National Institute of Health) from which vertebral body cross-sectional area (A; mm^2) and length (l; mm) were determined.

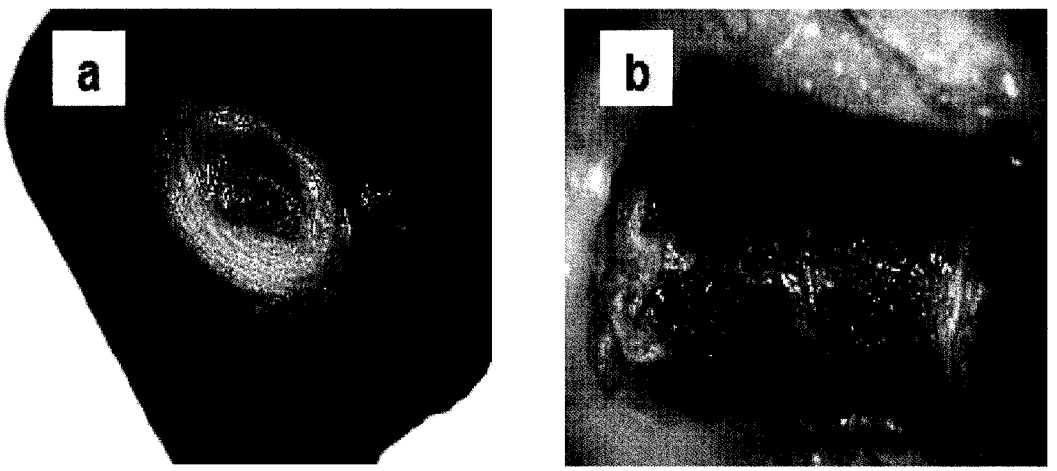

Figure 2-12: Digital images of vertebra in transverse (a) and coronal (b) planes

Once thawed, vertebrae were secured vertically into individual bolt heads using PMMA. PMMA was allowed to set for a minimum of 10 minutes and the bone was kept moist with saline soaked gauze throughout this period and up until testing.

Compression testing was performed on a mechanical testing machine (Instron 4465, Instron Canada) using a 1000N load cell. A stainless steel plate containing 19 holes, each 2.5 mm deep and differing 0.1 mm in diameter was placed beneath the load cell as shown in Figure 2-13. The purpose of this plate was to provide a tight fit with the distal end of each vertebra and prevent lateral movement and consequent shear forces on the bone. The desired hole was selected individually for each bone after which the bone-containing bolt was screwed into a connector on the load cell and the hole was clamped in place directly beneath the bone. The machine was then rebalanced.

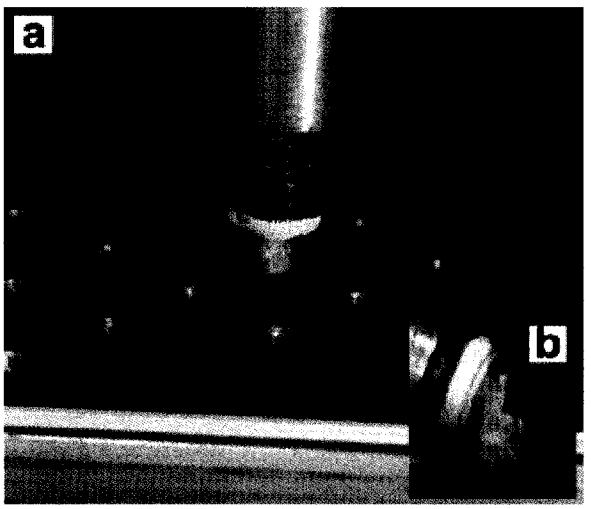

Figure 2-13: Vertebral compression a) bone arrangement in apparatus b) compression fracture

The vertebrae were loaded to 5 N to ensure contact on all sides of the hole as well as the bottom of the plate. Tests were then run at 1 mm/min, and data were collected every 0.1 seconds until an approximate 10% drop in failure load was observed. Load versus time data was acquired from the Instron by LabView data acquisition software. Time was converted into displacement data to construct a load-displacement curve. Figure 2-14 is a typical load-displacement curve from vertebral compression.

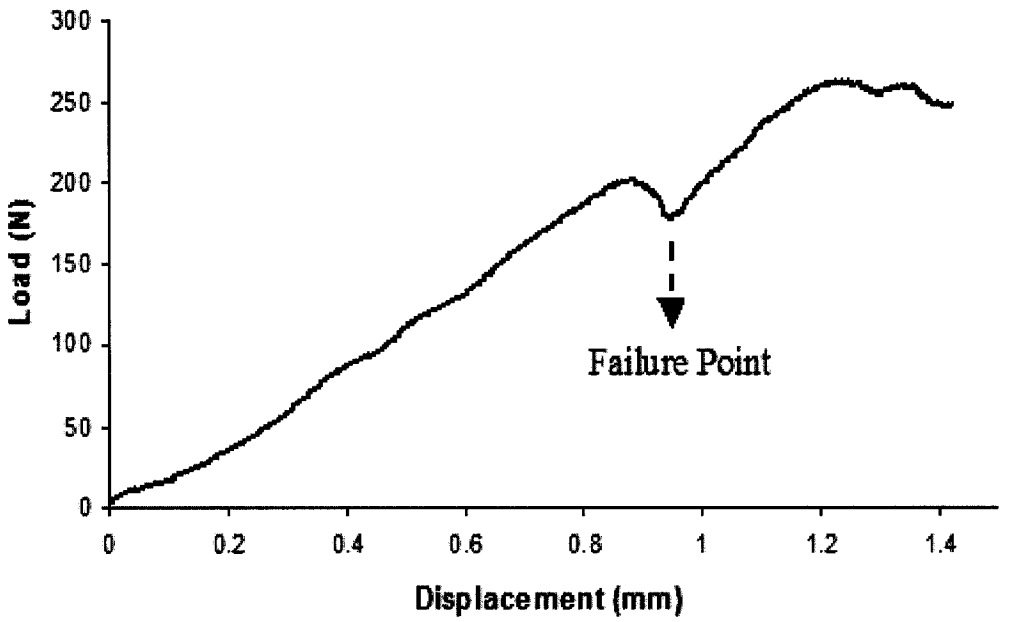

Figure 2-14: Typical load-displacement curve generated from vertebral compression

Cross-sectional area and vertebral height determined from the digital images were used to convert the load-displacement curve into a stress-strain curve. Normalized properties taken from the stress-strain curve included failure stress, failure strain, elastic modulus, and toughness. The formulae used to calculate the normalized parameters are as follows (Turner and Burr, 2001):

$$\sigma_f = \frac{F_f}{A_{cs}}$$

σ_f : *Failure stress* (MPa) [Equation 9]

F_f : *Bending moment* $(N \cdot mm)$

A_{cs} : *Cross – sectional area* (mm^2)

$$\varepsilon_f = \frac{\delta_f}{h_v} \cdot 100$$

ε_f : *Failure strain* (%) [Equation 10]

δ_f : *Displacement at failure* (*mm*)

h_v : *Height of vertebra* (*mm*)

$$E = \frac{h_v}{A_{cs}} K$$

E : *Elastic* modulus (*MPa*) [Equation 11]

h_v : *Height of the vertebra* (*mm*)

K : *Stiffness* (N/mm)

A_{cs} : *Cross* – sectional *area* (mm^2)

$$\mu_f = \sum_{j=1}^{n} (\sigma_{j-1})(\varepsilon_{j-1} - \varepsilon_j) + \left[\frac{(\sigma_{j-1} - \sigma_j)(\sigma_{j-1} - \sigma_j)}{2} \right]$$

μ_f : *Toughness* (mJ/mm^3)

σ : *Stress* (*MPa*) [Equation 12]

ε : *Strain*

n : *Total number of data* points *to yield*

j : *Integer increments from* 1 *to* n

2.5.4 Femoral Neck Fracture

The femoral neck region of the proximal end of the excised right femur was tested to evaluate the mechanical properties at a clinically-relevant and sensitive site. The femoral neck has a complex geometry and consists of a combination of both trabecular and cortical bone. Since the distal ends of the right femora were previously embedded in epoxy blocks for geometrical analysis, the proximal half up to the midshaft was available for testing.

Samples were removed from the freezer two hours before testing to ensure that they were thawed. Immediately before testing, the samples were secured into a testing jig. This jig consisted of a stainless steel tube with a hole bored into it for the bone to sit in and set screws to hold the bone vertical during set-up. Loading the bone into this jig piece first involved greasing the jig chuck with Vaseline and placing a square of cardboard in the base to simplify removal. The bone was then placed in the jig with the severed side down and the four screws were tightened to secure the bone in position. Following this, PMMA was pressed into the jig chuck surrounding the bone to tightly seal it. The PMMA was left to dry for 10 minutes prior to testing and during this period the bone was covered in saline soaked gauze.

Femoral neck fracture tests were performed on a mechanical testing machine (Instron 4465, Instron Canada Inc.) with a 1000 N load cell. The jig containing the bone was secured to the load cell and the machine was calibrated and balanced. A plate with a hole drilled out of it was placed beneath the top jig in a position that would facilitate contact only between the plate and the femoral head as shown in Figure 2-15. A preload

of approximately 1.0 N was applied. The test was run at 2.5 mm/min and load versus time data were collected every 0.1 seconds by LabView until failure.

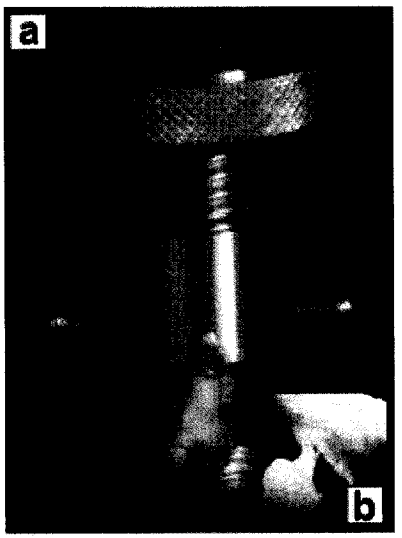

Figure 2-15: Femoral neck fracture testing a) bone arrangement in apparatus b) femoral neck fracture

Time was converted into displacement data to construct a load-displacement curve (see Figure 2-16). From this curve unnormalized mechanical properties were determined including failure load, failure deformation point, energy to failure and stiffness. These mechanical properties were compared directly without any normalization due to complicated loading and geometry.

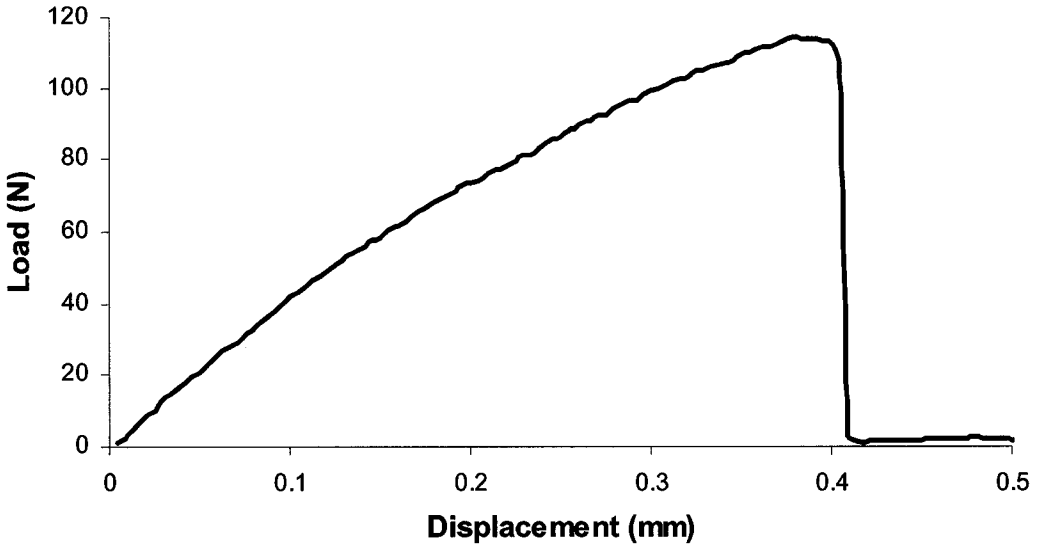

Figure 2-16: Typical load-displacement curve generated from femoral neck fracture testing

2.6 Evaluation of Bone Remodeling

Bone remodelling can be assessed *ex vivo* by various staining techniques on sections of bone tissue. Histomorphometry is the quantitative study of the microscopic structure of a tissue, specifically by computer-assisted analysis of data from stained images acquired via a microscope. Static histomorphometry is used to determine the relative amount of unmineralized bone (osteoid) versus mineralized bone in the tissue section (Eriksen *et al.*, 1994).

2.6.1 Static Histomophometry

Static histomorphometry was performed on undecalcified blocks of the promixal tibia to evaluate bone morphology, generating quantitative data on bone structure and formation.

The right tibia was stored in 70% ethanol after dissection. The tibias were sectioned coronally, exposing the marrow using a low speed bone saw (Isomet, Bueler). Proximal cranial sections were then inserted into individual cassettes and placed in 70% ethanol for an additional week. Following this, the samples were dehydrated in ascending concentrations of acetone and subsequently infiltrated in ascending ratios of unpolymerized Spurr resin and acetone. The bones were finally embedded in blocks of Spurr resin that was polymerized in a 60°C over for 48 hours.

The spurr embedded tibiae blocks were sectioned using a semi-automatic microtome (Reichert-Jung 2050). Three sequential 5 μm sections and one 7 μm section were taken from each block and placed in 60°C waterbath with 1 tablespoon of 100 bloom gelatin added. Sections were then positioned onto gelatinized slides and a plastic cover was smoothed over the sections to remove air bubbles. Siliconized slides were sandwiched between the sample slides. All slides from an individual block were stacked, clamped together and placed in a 65°C over for 48 hours.

Individual 5 μm sections were stained with Goldner's Trichrome (Schenk *et al.*, 1994), which stains mineralized bone blue/green and osteoid red/orange. An example of a section of proximal tibia tissue stained with Goldner's Trichrome is illustrated in Figure 2-17a. Sections were analysed under a 10x objective lens, using a computer image analysis system consisting of a Zeiss microscope attached to a video camera (Retiga 1300), which acquired the image and transmitted it onto the computer monitor. Bioquant morphometry program computer software (Bioquant Nova Prime, version 6.50.10) was used to quantify the static histomorphometry parameters. All measurements were performed on the computer screen using the acquired image of the section

Sections were measured 1mm or 1 field width under the growth plate and 1 mm from the cortical bone. This was to ensure measurement of only trabecular bone and not the intermediary zone (Fawcett, 2004). Eight serial fields were analysed for each proximal tibia section, as seen in Figure 2-17b. The structural and bone formation parameters measured (Table 2-2) were done so in accordance with the standard nomenclature of bone histomorphometry as stated by the American Society for Bone and Mineral Research (Parfitt *et al.*, 1987).

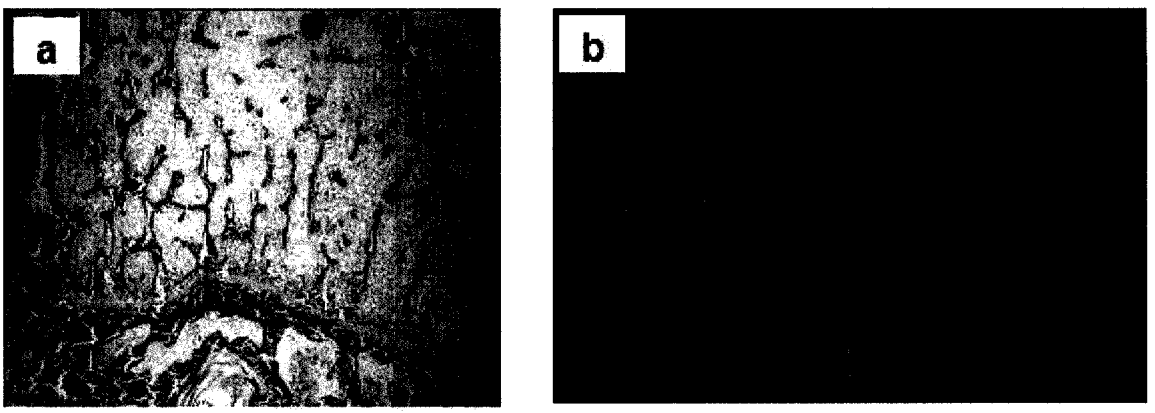

Figure 2-17: Histomorphometry technique (a) Proximal tibia section stained with Goldner's trichrome; (b) topographical map displaying fields quantified using Bioquant morphometry system

Table 2-2: Structural and formation parameters generated from static histomorphometry

	Parameter	Abbreviation	Formula	Unit
Structural Parameters	Trabecular Bone Volume	%TBV	BV/TV	%
	Trabecular Thickness	Tb.Th.	BV/BS	μm
	Trabecular Number	Tb.N.	(BV/TV)/Tb.Th. x 1000	mm^{-1}
	Trabecular Separation	Tb.Sp.	(1000/Tb.N) - Tb.Th.	μm
Formation Parameters	Osteoid Volume	%OV	OV/BV	%
	Osteoid Surface	OS/BS	OS/BS	%
	Osteoid Thickness	O.Th.	OV/OS	μm
Resorption Parameters	Eroded Surface	ES	ES/BS	%

where BV is bone volume, TV is tissue volume, BS is bone surface, OV is osteoid volume and OS is osteoid surface.

2.7 Evaluation of Bone Structural Properties

Bone structural properties can be assessed by the overall trabecular microarchitecture and trabecular connectivity. An insight into the connectivity of the trabecular network can be gained through strut analysis on 2D bone images. The determination of both structural and connectivity parameters is essential, as a sample may have a lot of bone mass (high %TBV) but it may be very poorly connected; this poor connectivity may in turn adversely affect the bone mechanical properties.

2.7.1 Strut Analysis

Strut analysis was performed on back scattered electron (BSE) images of spurr embedded tibia, which previously had sections removed for histomorphometric analysis (see Section 2.6.1). In these images, mineralized bone appears grey or white while unmineralized bone and spurr appear black. Similar to histomorphometric analysis, the trabecular bone area below the growth plate and within the cortex was analysed. The images were analysed on a Quantimet 500 IW system using the program Quips, written by Dr. Dimitriu. The program identified structural parameters including trabecular bone volume, trabecular thickness, trabecular number and trabecular separation. Connectivity parameters including nodes, free ends, node-node struts, node-free end struts, and free-free struts (see Figure 2-18) were also determined.

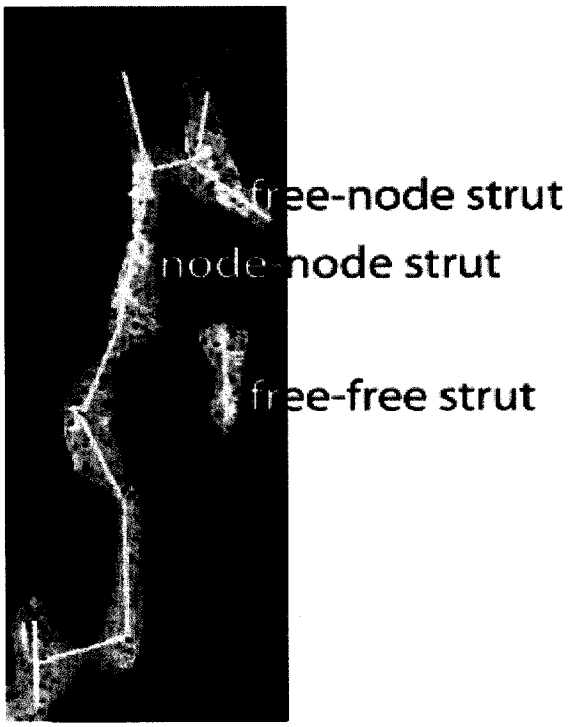

Figure 2-18: Identification of node-node, free-node and free-free struts

2.8 Evaluation of Bone Mineral Properties

Two well-characterized methods use to evaluate mineral quality are quantitative Back Scattered Electron (qBSE) imaging and microhardness testing. BSE imaging generates a distribution of the mineralization values over a cross-section of local bone area. Compared to bone mineral density measurements, BSE allows one to speculate on the "age" of the mineral distribution and its level of homogeneity within a given area (Grynpas, 1993; Reid and Boyde, 1987). Microhardness testing on the other hand is used to measure the resistance of a material to indentation. As bone consists of two major components, one (mineral) which is considerably harder than the other (collagen), the microhardness of the composite material reflects their proportions; in other words, the degree of mineralization of the bone.

2.8.1 Quantitative Back Scattered Electron (qBSE) Imaging

The spurr embedded tibiae, which previously had sections removed for histomorphometric analysis, were used for evaluation of mineralization distribution using Back Scattered Electron (BSE) imaging. In preparation for BSE imaging, the surface of each block was ground on 400 grade grinding paper followed by 600 grade and 1200 grade. Blocks were then polished using a 6 μm and a 1 μm diamond polish. Polishing was performed on a Pheonix BETA Grinder/Polisher. Using Fimo (Fimo Classic, Eberhard Faber) the blocks were then mounted on plexiglass plates in groups of 5 and made level to each other. Plates were wrapped in carbon tape and carbon-coated, and imaged using BSE imaging (solid state BSE detector, FEI Company, Hillsboro, OR, USA) on a FEI XL300ESEM. Beam conditions were set at 20 kV, the working distance of 15 mm, and spot size of 7.

A scanning electron microscope works through a focused beam that is continuously scanned, in a raster-like pattern, over the surface of a specimen. This scanning causes backscatter of some of the primary electrons and ejection of secondary electrons. The backscattered electrons are collected and may be used to detect contrast between regions of different chemical compositions, namely through differences in average atomic number. Regions containing higher atomic numbers have an increased probability of collisions with these electrons. The intensity of electron collisions is not only related to atomic number, but also to the density of the atomic nuclei. Thus, an area of bone that has a greater density of calcium atomic nuclei will display a greater intensity of electron collisions.

The relative backscattering of mineralized tissues were determined by comparison with a silicon dioxide (SiO_2) standard, which was measured between every sample. This was required to correct for the variation (drift of the machine) that could potentially occur between specimens. Four fields per sample were taken (80x magnification) and ultimately stitched together as illustrated in Figure 2-19a. A mask was created over this base image to isolate cortical and trabecular regions. Both the spur resin and the unmineralized bone appeared black. The grey sections reflected bone with varying degree of mineralization where dark grey represented low mineralization and white represented a high degree of mineralization.

Histograms of the grey level distributions of cortical and trabecular bone were created, with increasing grey levels representing a higher degree of mineralization (Boyde and Jones, 1983) (see Figure 2-19b). Shifts in mineralization profiles were compared using a cumulative log ratio known as the logit function (Lundon *et al.*, 1994):

$$\text{logit} = \ln \frac{area \leq cutoff}{area > cutoff} \qquad \text{[Equation 13]}$$

Where "area" refers to the total bone fraction area defined within a specific mineralization range, and "cutoff" values were chosen relative to the average grey level within a specific control group. A cutoff value of 149 (average trabecular bone mineralization peak for OVX group) was chosen for the analysis of trabecular bone mineralization, while a cutoff value of 161 (average cortical bone mineralization peak for OVX group) was chosen for the analysis of cortical bone. The closer the logit function is to zero, the more normally distributed the mineralization profile appears. Negative logit functions represent skewed hypermineralized distributions, while positive logit functions represent skewed hypomineralized distributions. The grey level corresponding to the

peak intensity was also noted, as well as the full width at half the maximum height (FWHMH) of each histogram, which represents the heterogeneity of the distribution.

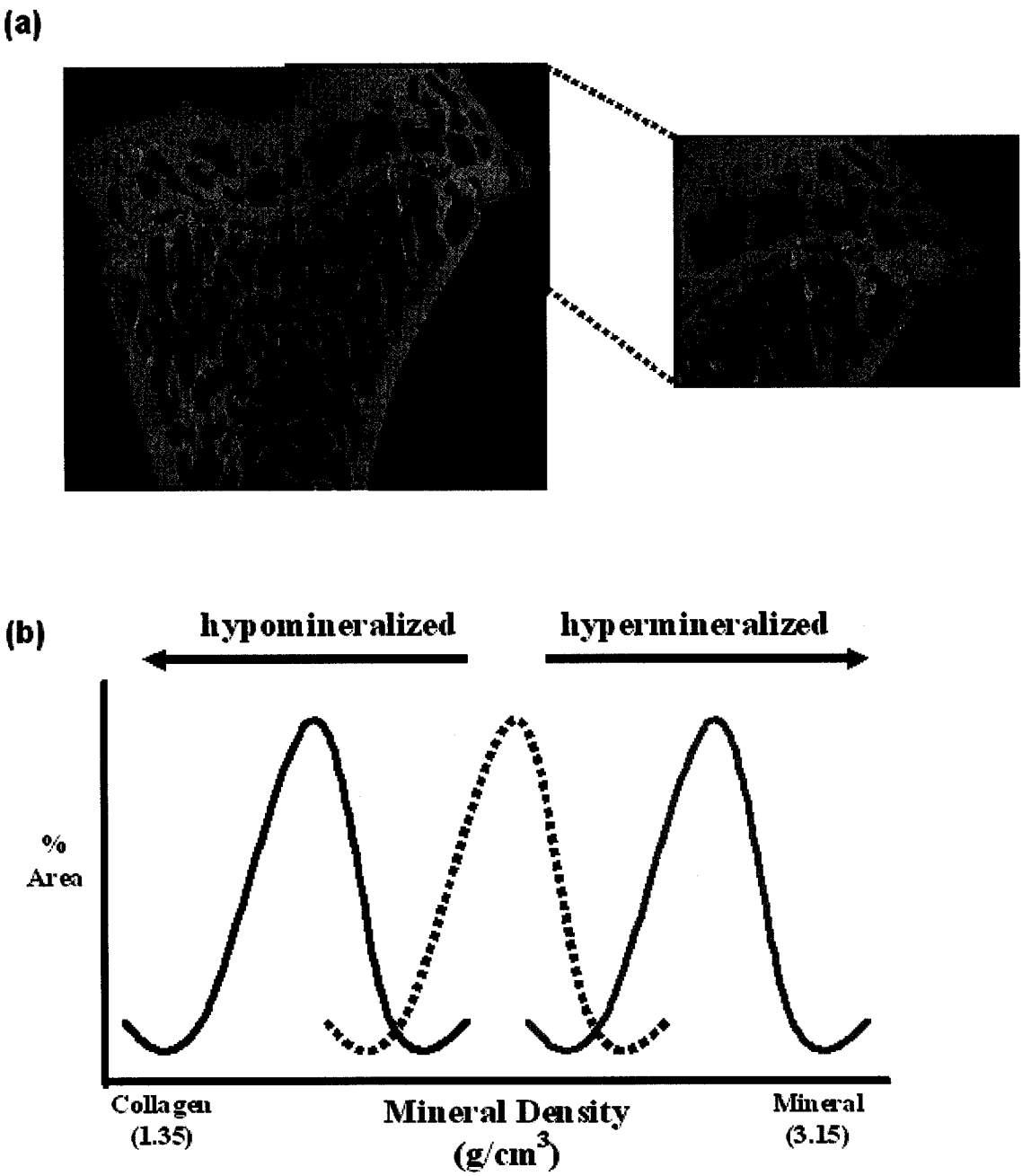

Figure 2-19: Quantitative back scattered electron imaging technique (a) BSE image of proximal tibia, with magnified subregion of trabeculae illustrating varying grey levels; (b) mineralization distributions as determined by quantitative BSE imaging

2.8.2 Microhardness

The spurr embedded tibiae, previously polished to 1 μm diamond finish and used for BSE, were hardness tested. These blocks were secured onto a small plastic Petri dish using Fimo (Fimo Classic, Eberhard Faber). Testing was performed on a Mitutoyo HM-122 microhardness tester (Mitutoyo, Japan) with a Vickers diamond indenter. The machined was zeroed before each test.

The dish containing the block was secured into the sample holder of the microhardness tester. Under a magnification of 20X the sample was aligned such that the point of interest would be directly under the indenter. Care was taken to avoid placement over cracks, edges, polishing scores and other imperfections. Once aligned, the specimen was indented with a load of 25g for 10s. The lengths of the indentation's two diagonals were then measured. Ten indents were made on the cortical bone (5 lateral, 5 medial) and ten indents were made on separate trabeculae. Average cortical and trabecular hardness were determined using the following equations:

$$Vickers\ Hardness\ (HV) = \frac{F}{gS}$$

F : *Test Force* (N) [Equation 14]
g : *Acceleration due to gravity* $(9.8\ m/s^2)$
S : *Surface area of indentation* (mm^2)

$$Surface\ Area\ of\ Indentation\ (mm^2) = \frac{1.854w}{D^2}$$

[Equation 15]

w : *Test weight*(g)
D : *Average legth of two diagonals*

2.9 Statistical Analysis

Statistical analysis was performed using statistical software SPSS (version 15.0). Comparisons involving two-groups were performed using an independent t-test. Multiple comparisons were performed using a one-way ANOVA with the pairwise comparison Protected Fisher's Least Significant Difference (LSD) post hoc test. A p-value less than 0.05 was considered significant while a p-value less than 0.1 was considered a trend. Damaged samples and extreme outliers (three standard deviations from the mean) were excluded from the analysis. All data is displayed as mean ± standard error of the mean (SEM).

Chapter 3 : Results

3 Introduction

This chapter presents the effects of AOD on the ovariectomized rat skeleton. Here we are attempting to understand if AOD can be anabolic to OVX-induced bone loss. Groups treated with AOD will be compared to OVX controls and in the case of changes will also be compared to normal controls. All data is expressed as mean ± standard error of mean (SEM). [a] reflects a significance of $p<0.05$ vs. OC while [b] reflects a significance of $p<0.05$ vs. NC. Meanwhile, [c] reflects a significance of $p<0.1$ vs. OC while [d] reflects a significance of $p<0.1$ vs. NC.

3.1 Bone Densitometry

Dual Energy X-Ray Absorptiometry (DXA) was performed on excised lumbar vertebrae (L4-6) and excised left femora. The OVX control had significantly lower femoral and vertebral BMD compared to the normal control (Table 3-1) indicating that OVX decreased the amount and density of cortical and trabecular bone. AOD administration, on the other hand, had no significant effect on femoral or vertebral BMD of the dosed groups compared to the OVX control.

Table 3-1: Bone Mineral Density (BMD) and Bone Mineral Content (BMC) of the Left Femur and L4, L5, and L6 Lumbar Vertebrae

Group	Femur	
	N	BMD (g/cm^2)
NC	16	0.209 ± 0.004^a
OC	13	0.195 ± 0.002^b
O(0.01)	13	0.191 ± 0.002^b
O(0.03)	14	0.192 ± 0.003^b
O(0.25)	14	0.195 ± 0.002^b

$^a p \leq 0.05$ versus OC $^b p \leq 0.05$ versus NC $^c 0.05 < p \leq 0.1$ versus OC $^d 0.05 < p \leq 0.1$ versus NC

Group	Lumbar Vertebrae (L4+L5+L6)	
	N	BMD (g/cm^2)
NC	16	0.112 ± 0.003^a
OC	12	0.096 ± 0.001^b
O(0.01)	13	0.094 ± 0.002^b
O(0.03)	14	0.091 ± 0.002^b
O(0.25)	14	0.094 ± 0.003^b

$^a p \leq 0.05$ versus OC $^b p \leq 0.05$ versus NC $^c 0.05 < p \leq 0.1$ versus OC $^d 0.05 < p \leq 0.1$ versus NC

3.2 Bone Mechanical Properties

To evaluate bone mechanical properties, four mechanical tests (three-point bending, torsion testing, vertebral compression and femoral neck fracture) were performed on all five groups. Results from both un-normalized and normalized data are presented. Since un-normalized data represent failure behaviour at the whole bone level, these are termed bone structural properties. Normalized data represent failure behaviour at the tissue level, and are therefore termed bone material properties. Geometric data are also presented on the right femora and fifth lumbar vertebrae, which were used for data normalization purposes.

3.2.1 Three-Point Bending

Geometric properties of the right femora are shown in Table 3-2. There were no significant differences in femoral length, external medial/later diameter, and polar moment of inertia between the AOD-dosed groups and the OVX control group. There was, however, a dose-dependent increase in the external anterior/posterior diameter, cortical thickness, cross-sectional area and moment of inertia with AOD treatment. This dose-dependent increase became significant over both control groups at AOD-0.25. The increase in these parameters with AOD treatment suggests that the new osseous tissue was deposited on the periosteal surface of the femur.

The results of three-point bending tests are shown in Table 3-3. There were no significant differences in structural properties between the AOD-dosed groups and the OVX control group. However, once normalized for differences in geometrical properties, it was evident that the O(0.25) group achieved significantly lower ultimate stress than

both the OVX and normal control groups. This may have been due to the increase in femoral cross-sectional geometry.

Table 3-2: Geometric properties of the right femora

Geometrical Properties	Groups									
	N	NC	N	OC	N	O(0.01)	N	O(0.03)	N	O(0.25)
Femoral Length (mm)	15	37.97 ± 0.18	13	37.96 ± 0.16	13	37.54 ± 0.23	13	37.89 ± 0.19	14	38.06 ± 0.21
External Medial/Lateral Diameter (mm)	15	4.01 ± 0.11	13	3.88 ± 0.07	13	4.02 ± 0.07	13	3.72 ± 0.06[b]	14	3.72 ± 0.06[b]
External Anterior/Posterior Diameter (mm)	15	2.90 ± 0.06	12	2.90 ± 0.03	13	2.96 ± 0.03	13	3.02 ± 0.05[b,c]	14	3.06 ± 0.04[a,b]
Cortical Thickness (mm)	15	0.52 ± 0.02	13	0.49 ± 0.01	13	0.45 ± 0.02[c,b]	13	0.57 ± 0.02[a,b]	14	0.57 ± 0.13[a,b]
Cross-Sectional Area (mm^2)	15	4.67 ± 0.11	13	4.81 ± 0.11	13	4.51 ± 0.15	13	4.95 ± 0.13	14	5.23 ± 0.12[a,b]
Moment of Inertia (mm^4)	15	3.94 ± 0.24	13	4.16 ± 0.17	13	4.02 ± 0.17	13	4.28 ± 0.23	14	4.69 ±0.19[b,c]
Polar Moment of Inertia (mm^4)	15	10.98 ± 0.68	13	10.80 ± 0.45	13	10.83 ± 0.36	13	10.28 ± 0.53	14	11.05 ± 0.40

[a] $p \leq 0.05$ versus OC [b] $p \leq 0.05$ versus NC [c] $0.05 < p \leq 0.1$ versus OC [d] $0.05 < p \leq 0.1$ versus NC

Table 3-3: Three-point bending (structural and material properties) results

Structural Properties	Groups									
	N	NC	N	OC	N	O(0.01)	N	O(0.03)	N	O(0.25)
Ultimate Load (N)	13	154.11 ± 3.05	13	149.86 ± 4.47	13	143.37 ± 3.97	12	149.41 ± 4.72	14	144.79 ± 7.67
Failure Displacement (mm)	15	0.505 ± 0.019[a]	13	0.669 ± 0.023[b]	13	0.647 ± 0.033[b]	13	0.664 ± 0.031[b]	13	0.690 ± 0.043[b]
Energy to Failure (mJ)	15	45.16 ± 3.64[a]	13	64.17 ± 3.89[b]	13	57.63 ± 4.63	13	63.85 ± 3.85[b]	14	68.84 ± 5.92[b]
Stiffness (N/mm)	14	503.32 ± 14.57	13	507.10 ± 22.26	13	476.25 ± 14.22	13	503.36 ± 30.75	14	487.79 ± 35.27

[a]p ≤0.05 versus OC [b]p ≤0.05 versus NC [c]0.05 < p ≤0.1 versus OC [d]0.05 < p ≤0.1 versus NC

Material Properties	Groups									
	N	NC	N	OC	N	O(0.01)	N	O(0.03)	N	O(0.25)
Ultimate Stress (MPa)	15	216.85 ± 12.07	13	209.02 ± 7.81	13	203.74 ± 4.94	13	211.74 ± 10.88	14	180.95 ± 8.46[a,b]
Failure Percent Strain (%)	15	3.69 ± 0.16[a]	13	4.85 ± 0.16[b]	13	4.55 ± 0.30[b]	13	4.95 ± 0.26[b]	13	5.16 ± 0.33[b]
Toughness (mJ/mm^3)	15	4.73 ± 0.40[a]	13	6.42 ± 0.32[b]	13	5.87 ± 0.47	13	6.59 ± 0.31[b]	14	6.63 ± 0.55[b]
Modulus (GPa)	15	10.29 ± 0.80	13	9.81 ± 0.55	13	9.55 ± 0.47	13	9.77 ± 0.99	14	8.40 ± 0.65

[a]p ≤0.05 versus OC [b]p ≤0.05 versus NC [c]0.05 < p ≤0.1 versus OC [d]0.05 < p ≤0.1 versus NC

3.2.2 Torsion Testing

The results of torsion tests are shown in Table 3-4. There was a significant decrease in angular displacement at failure of all three AOD-dosed groups versus the OVX control. Likewise, the angular displacement at failure of the normal control group was also significantly lower than that of the OVX control. In addition, a significant increase in stiffness was observed in all three AOD-dosed groups versus both OVX and normal controls.

Once normalized for differences in geometric properties, similar trends were observed. There was a significant decrease in shear failure percent strain in the O(0.03) and O(0.25) groups versus the OVX control while a trend to decrease shear failure percent strain was evident in the O(0.01) group. Similarly, the shear failure percent strain of the normal control group was significantly lower than that of the OVX control. Furthermore, the O(0.25) group had a significantly greater shear modulus compared to both OVX and normal controls, and trend to increase shear modulus was evident in the O(0.03) group compared to the OVX control. These results suggest that AOD administration may have increased the mineralization of cortical bone thus resulting in a lowered angular displacement at failure and shear failure percent strain, and a greater stiffness and modulus of the AOD-dosed groups.

Table 3-4: Torsion testing (structural and material properties) results

Structural Properties	Groups									
	N	NC	N	OC	N	O(0.01)	N	O(0.03)	N	O(0.25)
Failure Torque (N•mm)	15	321.08 ± 31.97	13	371.02 ± 35.45	11	444.11 ± 15.77[b]	13	402.71 ± 33.12	14	435.27 ± 33.22[b]
Angular Displacement at Failure (rad)	13	0.259 ± 0.017[a]	13	0.357 ± 0.035[b]	11	0.261 ± 0.019[a]	13	0.261 ± 0.020[a]	13	0.262 ± 0.016[a]
Energy to Failure (mJ)	14	47.52 ± 6.22[a]	13	66.49 ± 8.81[b]	11	56.83 ± 3.49	13	56.77 ± 5.87	14	60.03 ± 6.22
Stiffness (N•mm/rad)	15	1340.97 ± 133.95	13	1349.43 ± 140.62	11	2029.54 ± 145.44[a,b]	13	1796.35 ± 137.70[a,b]	14	1974.02 ± 172.18[a,b]

[a]p ≤0.05 versus OC [b]p ≤0.05 versus NC [c]0.05 < p ≤0.1 versus OC [d]0.05 < p ≤0.1 versus NC

Material Properties	Groups									
	N	NC	N	OC	N	O(0.01)	N	O(0.03)	N	O(0.25)
Shear Stress (MPa)	15	59.95 ± 6.92	13	67.17 ± 6.70	11	83.41 ± 2.77[b]	13	74.44 ± 6.11	14	68.44 ± 7.84
Shear Failure Percent Strain (%)	13	4.06 ± 0.29[a]	13	5.34 ± 0.47[b]	11	4.40 ± 0.39[c]	13	3.94 ± 0.29[a]	13	3.69 ± 0.19[a]
Toughness (mJ/mm^3)	15	0.92 ± 0.16	13	1.08 ± 0.13	11	1.09 ± 0.11	13	0.95 ± 0.10	14	0.87 ± 0.09
Shear Modulus (GPa)	15	1.68 ± 0.24	13	1.63 ± 0.19	11	2.28 ± 0.17[a]	13	2.21 ± 0.21[c]	14	2.39 ± 0.22[a,b]

[a]p ≤0.05 versus OC [b]p ≤0.05 versus NC [c]0.05 < p ≤0.1 versus OC [d]0.05 < p ≤0.1 versus NC

3.2.3 Vertebral Compression

The geometric properties of the sixth lumbar vertebrae used in compression testing are shown in Table 3-5. Interestingly, all three AOD-dosed groups had a significantly lower vertebral body height compared to the OVX and normal controls. Furthermore, all three AOD-dosed groups, as well as the normal control group, had a significantly decreased vertebral body cross-sectional area compared to the OVX control.

The results of vertebral compression tests are shown in Table 3-6. There was a significant increase in stiffness in the O(0.25) group compared to both OVX and normal controls. Furthermore, it is important to note that the value for ultimate load in the O(0.25) group was in between the ultimate load values of the OVX and normal controls; that is, the ultimate load of the O(0.25) group was not significantly different from either the OVX or normal control groups. This indicates that as the dose of AOD increased so did the maximum amount of force that can be placed on the vertebrae.

When normalized for differences in geometric properties, similar trends were observed. A trend to increase ultimate stress was evident at the highest dose of AOD versus the OVX control. Similarly, a trend to increase ultimate stress was also evident in the normal control group versus the OVX control. Furthermore, there was a significant increase in modulus in the O(0.25) group compared to both OVX and normal controls. These results suggest that AOD administration may have restored vertebral bone strength thus resulting in an increased ultimate stress. These results also suggest that AOD administration may have increased the mineralization of trabecular bone thus resulting in an increase in stiffness and modulus.

Table 3-5: Geometric properties of the sixth lumbar vertebae

Geometrical Properties	Groups									
	N	NC	N	OC	N	O(0.01)	N	O(0.03)	N	O(0.25)
Height of Vertebral Body (mm)	16	8.08 ± 0.17	7	8.03 ± 0.04	13	7.12 ± 0.21[a,b]	14	7.10 ± 0.16[a,b]	14	7.00 ± 0.10[a,b]
Cross-Sectional Area of Vertebral Body (mm^2)	16	12.33 ± 0.39[a]	12	13.75 ± 0.30[b]	13	12.18 ± 0.30[a]	12	11.24 ± 0.35[a,b]	14	11.72 ± 0.46[a]

[a] $p \leq 0.05$ versus OC [b] $p \leq 0.05$ versus NC [c] $0.05 < p \leq 0.1$ versus OC [d] $0.05 < p \leq 0.1$ versus NC

Table 3-6: Vertebral compression (structural and material properties) results

Structural Properties	Groups									
	N	NC	N	OC	N	O(0.01)	N	O(0.03)	N	O(0.25)
Ultimate Load (N)	15	195.74 ± 19.63	13	167.52 ± 15.16	13	137.47 ± 10.98[b]	13	141.71 ± 10.36[b]	14	181.36 ± 20.93
Failure Displacement (mm)	14	0.99 ± 0.08	12	1.17 ± 0.11	12	0.84 ± 0.12[a]	10	0.94 ± 0.07[c]	12	1.03 ± 0.07
Energy to Failure (mJ)	14	94.35 ± 15.23	13	88.80 ± 16.20	12	54.38 ± 7.87[b,c]	10	50.96 ± 5.89[a,b]	12	71.25 ± 9.97
Stiffness (N/mm)	16	323.49 ± 25.77	13	323.03 ± 32.92	13	312.82 ± 31.16	13	352.52 ± 27.82	14	438.83 ± 48.82[a,b]

[a]p ≤0.05 versus OC [b]p ≤0.05 versus NC [c]0.05 < p ≤0.1 versus OC [d]0.05 < p ≤0.1 versus NC

Material Properties	Groups									
	N	NC	N	OC	N	O(0.01)	N	O(0.03)	N	O(0.25)
Ultimate Stress (MPa)	15	15.50 ± 1.35[c]	13	11.78 ± 1.09[d]	13	11.72 ± 1.10[d]	13	13.24 ± 1.68	14	16.02 ± 2.17[c]
Failure Percent Strain (%)	14	12.57 ± 1.11	13	15.35 ± 1.59	12	11.23 ± 1.39[a]	10	13.73 ± 1.03	12	14.61 ± 1.02
Toughness (mJ/mm^3)	14	0.94 ± 0.14	13	0.80 ± 0.15	12	0.61 ± 0.08[d]	10	0.61 ± 0.09[d]	12	0.89 ± 0.16
Modulus (MPa)	16	208.81 ± 11.74	11	167.15 ± 9.01	13	182.21 ± 17.44	13	214.37 ± 19.74	14	269.11 ± 32.44[a,b]

[a]p ≤0.05 versus OC [b]p ≤0.05 versus NC [c]0.05 < p ≤0.1 versus OC [d]0.05 < p ≤0.1 versus NC

3.2.4 Femoral Neck Fracture

The results of femoral neck fracture tests are shown in Table 3-7. As stated in section 2.5.4, data from femoral neck fracture tests are typically only presented as un-normalized data due to the complex geometry and fracture angle generated by each specimen.

All three AOD-dosed groups achieved significantly lower ultimate loads compared to the OVX control group. This situation was similar to the normal control group in which there was a trend to decrease ultimate load compared to the OVX control group. In addition, the three-AOD dosed groups absorbed significantly less energy to failure compared to the OVX control group, but had similar energy to failure values as the normal control group. These results have to be considered with caution due to the very large variation in measurement, especially in the OVX group.

Table 3-7: Femoral neck fracture results (structural properties)

Structural Properties	Groups									
	N	NC	N	OC	N	O(0.01)	N	O(0.03)	N	O(0.25)
Ultimate Load (N)	14	113.73 ± 5.66[c]	12	127.89 ± 8.47[d]	13	102.28 ± 3.79[a]	13	106.48 ± 5.05[a]	14	97.76 ± 5.46[a,b]
Failure Displacement (mm)	14	0.53 ± 0.05[a]	12	0.72 ± 0.10[b]	13	0.58 ± 0.06	13	0.59 ± 0.05	14	0.45 ± 0.05[a]
Energy to Failure (mJ)	14	33.50 ± 5.03[a]	12	51.11 ± 9.49[b]	13	29.82 ± 2.80[a]	12	30.58 ± 7.74[a]	14	24.05 ± 2.59[a]
Stiffness (N/mm)	14	277.04 ± 19.96	12	284.52 ± 26.18	13	243.65 ± 13.50	13	226.25 ± 20.40[c,d]	14	264.44 ± 22.69

[a] $p \leq 0.05$ versus OC [b] $p \leq 0.05$ versus NC [c] $0.05 < p \leq 0.1$ versus OC [d] $0.05 < p \leq 0.1$ versus NC

3.3 Bone Remodeling

Bone remodeling was evaluated through histomorphometry. Histomorphometry results can be separated into two sets of properties: two-dimensional (2D) trabecular bone structural properties and trabecular bone formation properties.

3.3.1 Histomorphometry

The results of the trabecular bone structural properties are shown in Table 3-8. Substantial cancellous bone loss occurred in the OVX control group predominantly by a reduction in trabecular bone volume (%TBV) and trabecular number (Tb.N.), and an increase in trabecular separation (Tb.Sp.). The values for %TBV, Tb.N., and Tb.Sp. in the AOD-dosed groups were in between those of the OVX and normal controls. O(0.03) and O(0.25) had values for %TBV that were significantly higher than the OVX control yet, at the same time, significantly lower than the normal control. Similarly, a trend to increase Tb.N. was evident in the O(0.03) and O(0.25) groups compared to the OVX control, yet Tb.N. was significantly lower in these groups compared to the normal control. With regards to Tb.Sp., all three AOD-dosed groups had values significantly lower than the OVX control, and at the same time significantly higher than the normal control. These results indicate that AOD may have partially recovered some of the OVX-induced loss of trabecular structure.

The results of the trabecular bone formation properties are also shown in Table 3-8. The marked osteopenia in OVX rats was associated with increased indexes of bone formation (osteid volume and osteoid surface). O(0.03) and O(0.25) had osteoid surface (OS/BS) values that were significantly lower than the OVX control and similar to the

normal control. Furthermore, AOD administration resulted in a dose-dependent decrease in osteoid volume (%OV) over the OVX control. Nonetheless, AOD-0.25 maintained a significantly ($p=0.093$) higher %OV over the normal control. These results indicate that AOD may have reduced some of the OVX-induced increases in bone formation while still maintaining an anabolic effect on bone.

Table 3-8: Histomorphometry results (structural, formation and resorption properties) for proximal tibiae

Structural Properties	Groups									
	N	NC	N	OC	N	O(0.01)	N	O(0.03)	N	O(0.25)
%TBV (%)	16	13.50 ± 1.49[a]	13	6.42 ± 0.85[b]	12	7.35 ± 0.85[b]	13	9.83 ± 0.96[a,b]	13	9.49 ± 0.96[b,c]
Tb.Th. (μm)	16	97.56 ± 4.84	13	103.78 ± 5.52	13	109.39 ± 6.66	13	115.57 ± 6.78[b]	13	111.83 ± 6.06[d]
Th.N. (mm^{-1})	16	1.33 ± 0.16[a]	13	0.60 ± 0.06[b]	13	0.74 ± 0.08[b]	13	0.85 ± 0.07[b,c]	13	0.86 ± 0.09[b,c]
Tb.Sp. (μm)	15	689.19 ± 61.64[a]	13	1866.81 ± 263.37[b]	13	1403.59 ± 136.14[a,b]	10	930.35 ± 40.47[a]	13	1174.76 ± 106.39[a,b]

[a]p ≤0.05 versus OC [b]p ≤0.05 versus NC [c]0.05 < p ≤0.1 versus OC [d]0.05 < p ≤0.1 versus NC

Properties		Groups								
		N	NC	N	OC	N	O(0.01)	N	O(0.03)	N	O(0.25)
Formation	%OV (%)	16	0.15 ± 0.04[a]	12	0.48 ± 0.12[b]	13	0.51 ± 0.09[b]	13	0.34 ± 0.07	13	0.35 ± 0.09[d]
	OS/BS (%)	16	4.10 ± 1.23[a]	13	8.67 ± 1.99[b]	13	6.55 ± 1.18	13	4.32 ± 0.66[a]	13	4.43 ± 0.98[a]
	O.Th. (μm)	16	6.63 ± 0.83	13	7.43 ± 0.44	13	7.24 ± 0.24	13	7.38 ± 0.42	13	7.39 ± 0.29
Resorption	ES (%)	15	1.87 ± 0.43	13	1.67 ± 0.42	13	1.72 ± 0.39	13	1.18 ± 0.34	13	2.20 ± 0.54

[a]p ≤0.05 versus OC [b]p ≤0.05 versus NC [c]0.05 < p ≤0.1 versus OC [d]0.05 < p ≤0.1 versus NC

3.4 Bone Connectivity Properties

Trabecular bone structural properties were evaluated by strut analysis. This technique, which provides insight into trabecular connectivity, was performed on BSE images of spurr embedded tibia. Strut analysis results can be separated in measures of bone connectivity and measures of bone disconnectivity.

3.4.1 Strut Analysis

The results of the trabecular bone strut analysis are shown in Table 3-9. No significant differences were evident in any of the measured parameters between the AOD-dosed groups and the OVX control group; that is, according to strut analysis, AOD appeared to have no effect on the OVX-induced deterioration of bone structure. Nonetheless, in all parameters measured (excluding free-free strut length) the normal control group had significantly higher values than the OVX control group.

Table 3-9: Strut analysis results (connectivity properties) for proximal tibiae

	Properties	Groups									
		N	NC	N	OC	N	O(0.01)	N	O(0.03)	N	O(0.25)
Measures of Connectivity	Total strut length (mm/mm^2)	15	2.31 ± 0.20[a]	13	1.23 ± 0.10[b]	13	1.42 ± 0.14[b]	14	1.17 ± 0.09[b]	14	1.36 ± 0.14[b]
	Number of nodes (mm^{-2})	15	3.41 ± 0.47[a]	13	1.70 ± 0.21[b]	13	1.68 ± 0.22[b]	14	1.10 ± 0.12[b]	14	1.32 ± 0.15[b]
	Length of node-node struts (mm/mm^2)	15	0.66 ± 0.12[a]	13	0.21 ± 0.05[b]	13	0.30 ± 0.09[b]	14	0.18 ± 0.03[b]	14	0.18 ± 0.03[b]
	Length of free-node struts (mm/mm^2)	15	0.68 ± 0.08[a]	13	0.35 ± 0.04[b]	13	0.46 ± 0.08[b]	14	0.35 ± 0.05[b]	14	0.34 ± 0.06[b]
Measures of Disconnectivity	Number of free ends (mm^{-2})	15	6.35 ± 0.31[a]	12	3.89 ± 0.30[b]	13	4.21 ± 0.27[b]	14	4.57 ± 0.27[b]	14	4.49 ± 0.28[b]
	Length of free-free struts (mm/mm^2)	15	0.36 ± 0.05	13	0.26 ± 0.04	13	0.28 ± 0.03	14	0.32 ± 0.05	14	0.38 ± 0.04[c]

[a] $p \leq 0.05$ versus OC [b] $p \leq 0.05$ versus NC [c] $0.05 < p \leq 0.1$ versus OC [d] $0.05 < p \leq 0.1$ versus NC

3.5 Bone Mineral Properties

Bone mineral properties were evaluated by two methods: quantitative back scattered electron (qBSE) imaging to evaluate mineralization distributions in a representative 2D bone section and microhardness testing to evaluate the degree of mineralization of cortical and trabecular bone. qBSE was performed on polished Spurr blocks of proximal tibiae. Mineralization distributions of a defined trabecular bone area directly below the growth plate and of the outer cortical shell were determined. Microhardness testing was also performed on Spurr blocks of proximal tibiae. Ten indents were made on the outer cortical shell and ten indents were made on separate subchondral trabeculae.

3.5.1 Quantitative Back Scattered Electron Imaging

3.5.1.1 Quantitative Back Scattered Electron Imaging of Trabecular Bone

The average mineralization profiles for trabecular bone of the proximal tibia are shown in Figure 3-1. The quantitative BSE parameters are shown in Table 3-10. While OVX resulted in a shift towards lower mineralization, it was evident that the highest AOD dose (0.25 mg/kg/day) shifted the mineralization profile of the O(0.25) group 2.6% to higher grey levels as compared to the OVX control. This shift was also reflected in the logit function; as the dose of AOD increased, the logit beccame increasingly negative, representing a more hypermineralized distribution. Nonetheless, even at the highest dose of AOD, the shift in logit was not significantly different compared to the OVX control. It is important to note however, that the values for maximum grey level in the O(0.03) and O(0.25) groups were in between those of the OVX and normal controls, and were not

significantly different from either control group. Needless to say, the maximum grey level values for the OVX and normal controls were significantly different from each other, with the normal control group having a significantly higher maximum grey level and a more hypermineralized distribution. This indicates that at the highest dose of AOD, the mineralization profile of trabecular bone is no longer significantly different versus the normal control. Furthermore, there were negligible changes in the heterogeneity of the mineralization profiles amongst the five groups.

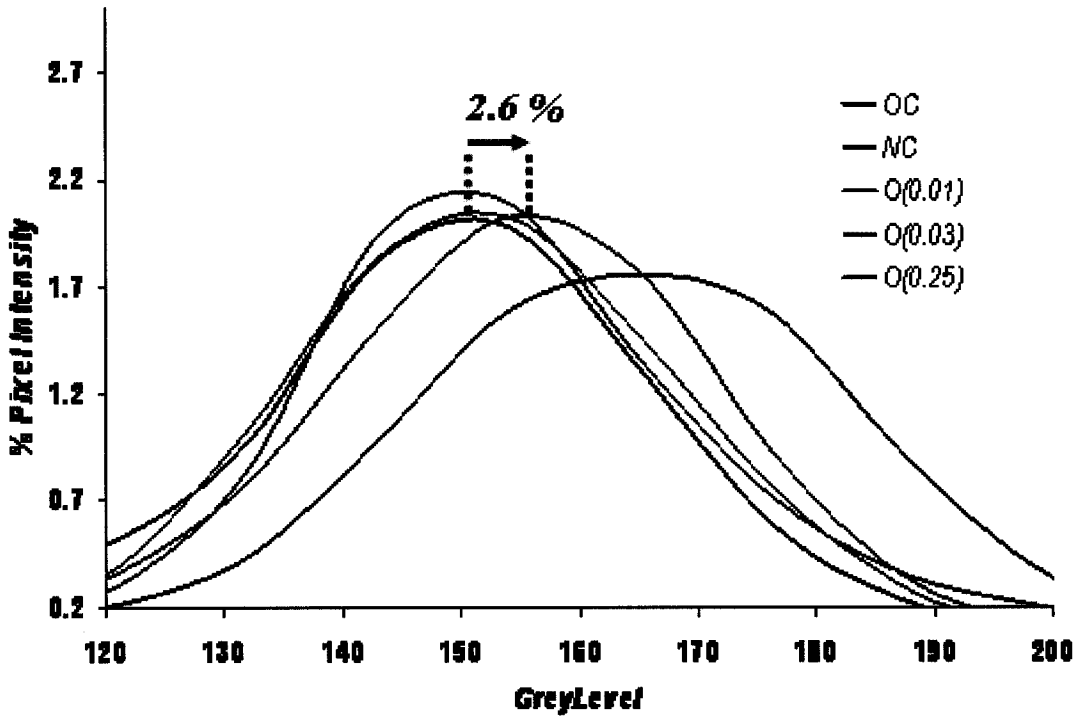

Figure 3-1: BSE distribution curves: comparing trabecular bone mineralization in O(0.01), O(0.03), O(0.25), OC, and NC groups

Table 3-10: Quantitative Back Scattered Electron Imaging of trabecular bone in the proximal tibia of AOD treated OVX rats

Group	N	Trabecular Bone		
		Logit (-)	Maximum Grey Level (pixels)	Level of Heterogeneity (pixels)
NC	15	-0.970 ± 0.231[a]	163.00 ± 2.92[a]	26.07 ± 0.88
OC	12	0.004 ± 0.291[b]	148.67 ± 4.31[b]	25.67 ± 0.78
O(0.01)	13	0.049 ± 0.283[b]	152.15 ± 3.03[b]	24.38 ± 0.87
O(0.03)	14	-0.190 ± 0.248[b]	155.50 ± 3.66	22.67 ± 0.63[a,b]
O(0.25)	13	-0.312 ± 0.297[d]	155.38 ± 2.70	24.29 ± 0.79

[a]$p \leq 0.05$ versus OC [b]$p \leq 0.05$ versus NC [c]$0.05 < p \leq 0.1$ versus OC [d]$0.05 < p \leq 0.1$ versus NC

3.5.1.2 Quantitative Back Scattered Electron Imaging of Cortical Bone

The average mineralization profiles for cortical bone of the proximal tibia are shown in Figure 3-2. The quantitative BSE parameters are shown in Table 3-11. While OVX resulted in a shift towards lower mineralization, it was evident that the highest AOD dose (0.25 mg/kg/day) shifted the mineralization profile of the O(0.25) group 2.3% to higher grey levels as compared to the OVX control. This shift was also reflected in the logit function; as the dose of AOD increased, the logit became increasingly negative, representing a more hypermineralized distribution. Nonetheless, even at the highest dose of AOD, the shift in logit was not significantly different compared to the OVX control. It is important to note however, that the values for maximum grey level in the O(0.03) and O(0.25) groups were in between those of the OVX and normal controls, and were not significantly different from either control group. Needless to say, the maximum grey level values for the OVX and normal controls were significantly ($p<0.1$) different from

each other, with the normal control group having a higher maximum grey level and a more hypermineralized distribution. This indicates that at the highest dose of AOD, the mineralization profile of cortical bone is no longer significantly different versus the normal control. Furthermore, there were negligible changes in the heterogeneity of the mineralization profiles amongst the five groups.

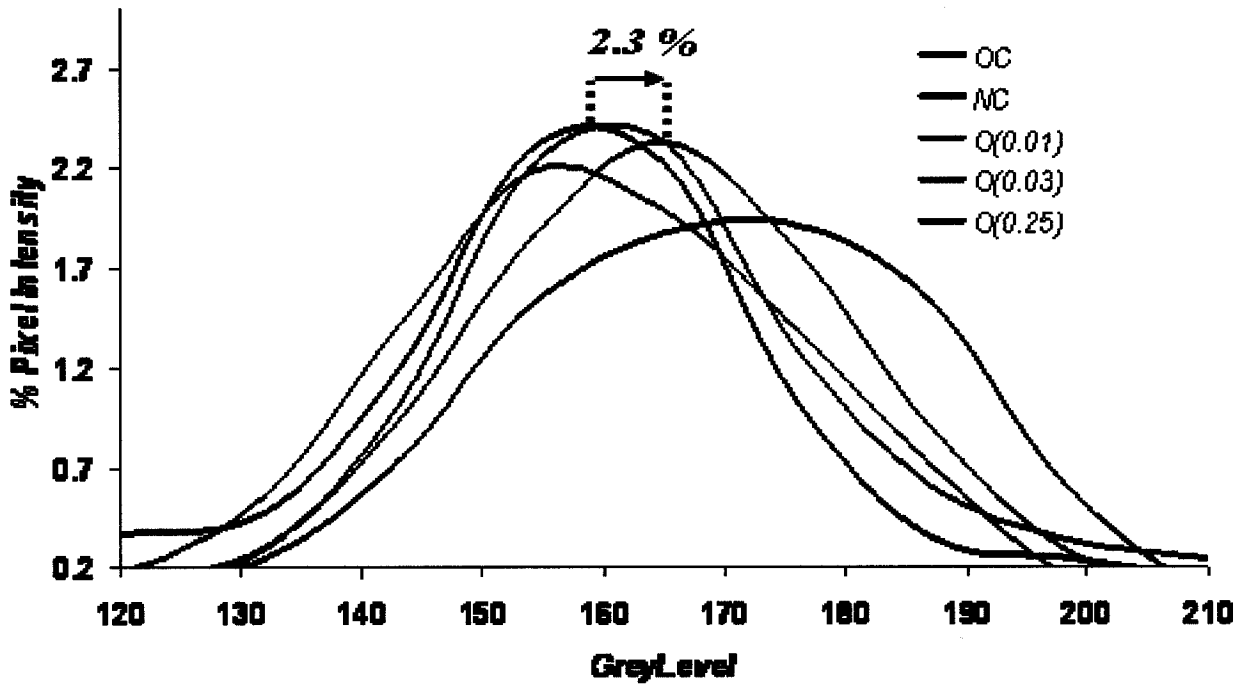

Figure 3-2: BSE distribution curves: comparing cortical bone mineralization in O(0.01), O(0.03), O(0.25), OC, and NC groups

Table 3-11: Quantitative Back Scattered Electron Imaging of cortical bone in the proximal tibia of AOD treated OVX rats

Group	N	Cortical Bone		
		Logit (-)	Maximum Grey Level (pixels)	Level of Heterogeneity (pixels)
NC	15	-0.690 ± 0.415	169.67 ± 3.55[c]	20.87 ± 0.68
OC	12	0.057 ± 0.458	159.08 ± 5.29[d]	22.38 ± 1.22
O(0.01)	13	0.541 ± 0.492[b]	160.08 ± 3.39	20.23 ± 0.58
O(0.03)	14	-0.100 ± 0.354	166.50 ± 4.19	20.79 ± 0.77
O(0.25)	13	-0.250 ± 0.374	165.08 ± 2.94	22.36 ± 1.06

[a]$p \leq 0.05$ versus OC [b]$p \leq 0.05$ versus NC [c]$0.05 < p \leq 0.1$ versus OC [d]$0.05 < p \leq 0.1$ versus NC

3.6 Microhardness Testing

The microhardness testing results are shown in Table 3-12. No significant differences were evident in the average hardness of cortical or trabecular bone amongst the five groups.

Table 3-12: Hardness of outer cortical shell of the and of the subchondral trabecular bone of the proximal tibia

Group	Cortical Bone	
	N	Average Hardness
NC	15	67.35 ± 2.08
OC	12	67.61 ± 1.24
O(0.01)	12	70.81 ± 1.12
O(0.03)	13	64.24 ± 1.91
O(0.25)	14	66.27 ± 2.18

[a]p ≤0.05 versus OC [b]p ≤0.05 versus NC [c]0.05 < p ≤0.1 versus OC [d]0.05 < p ≤0.1 versus NC

Group	Trabecular Bone	
	N	Average Hardness
NC	15	65.07 ± 1.64
OC	13	64.73 ± 2.02
O(0.01)	13	61.27 ± 1.42
O(0.03)	13	64.17 ± 2.89
O(0.25)	14	61.68 ± 1.98

[a]p ≤0.05 versus OC [b]p ≤0.05 versus NC [c]0.05 < p ≤0.1 versus OC [d]0.05 < p ≤0.1 versus NC

3.7 Summary of Results

Bone Mineral Density

- Significantly lower femoral and vertebral BMD was evident in the OVX control over the normal control
- AOD administration had no significant effect on femoral or vertebral BMD of the dosed groups compared to the OVX control

Mechanical Testing

- AOD treatment resulted in a dose-dependent increase in cross-sectional area, external anterior-posterior diameter, moment of inertia and cortical thickness that became significant over the OVX and N control at AOD-0.25
- In three-point bending, AOD-0.25 achieved significantly lower ultimate stress than both OVX and normal controls
- In torsion, modulus was significantly increased in AOD-0.25 over both OVX and normal controls
- In vertebral compression, AOD treatment resulted in a dose-dependent increase in ultimate stress and modulus that became significant over the OVX control at AOD-0.25

Histomorphometry

- The OVX control had a significantly reduced %TBV and Tb.N. and a significantly increased Tb.Sp. over the N control
- The values for %TBV, Tb.N., and Tb.Sp. in the AOD-dosed groups were in between those of the OVX and normal controls.
- %OV and OS/BS were significantly increased in the OVX group over the N group
- AOD administration resulted in a dose-dependent decrease in OS/BS over the OVX control
- AOD treatment resulted in a dose-dependent decrease in %OV over the OVX control.
- However, AOD-0.25 maintained a significantly ($p=0.093$) higher %OV over the normal control.

Back-scattered Electron Imaging

- OVX, O(0.01) and O(0.03) had significantly decreased mineralization over the N control
- At the highest dose of AOD, the mineralization profiles of cortical and trabecular bone are no longer significantly different versus the normal control

Chapter 4 : Discussion

4 Introduction

This study focused on the ability of AOD to rebuild the bone lost during ovariectomy (OVX) in a rat model of postmenopausal osteoporosis. Bone quality was evaluated through densitometry, mechanical testing, and techniques to assess remodeling, structural and material properties.

We found that AOD partially reversed to effects of OVX on trabecular bone but not cortical bone mechanical properties despite the fact that AOD treatment increased cortical bone mass via periosteal apposition at the femoral diaphysis. Furthermore, we found that AOD partially restored trabecular bone architecture and decreased remodeling over the OVX control. Lastly, we showed that AOD increased mineralization of cortical and trabecular bone and therefore suggest that AOD may have an anti-resorptive effect in addition to its anabolic effect.

Additional studies are required to further investigate the anabolic effect of AOD on the skeleton. There were many methodological issues to be addressed at the end of this study, which are discussed further in this chapter.

4.1 Current Anabolic Agents

Osteoporosis, a major worldwide health problem, affects 4 million to 6 million women and 1 million to 2 million men in North America (Canalis *et al.*, 2007). Even more people have a decreased bone mass, which, in addition to other risk factors, can be a major therapeutic challenge. Fractures, the most important consequence of osteoporosis, are associated with enormous costs and substantial morbidity and mortality. The prevention and treatment of this disease are therefore of paramount importance.

Since postmenopausal osteoporosis is characterized by bone resorption that exceeds bone formation, antiresorptive agents can help to restore skeletal balance by reducing bone turnover, primarily at the tissue level. Another therapeutic approach is anabolic – namely, to enhance bone formation. Anabolic agents differ fundamentally from antiresorptive drugs in their primary mechanism of action; that is, they directly stimulate bone formation. These bone formation stimulators include growth hormone (GH), insulin-like growth factor-I (IGF-I), and, above all, parathyroid hormone (PTH).

The most promising anabolic agent to date is PTH. PTH is currently available for clinical use as the recombinant human PTH (1-34) fragment known as teriparatide. Teriparatide appears to have all the classical anabolic properties as the full length PTH molecule. The beneficial effects of teriparatide on microarchitecture and bone geometry are clearly seen in the cancellous skeleton. Histomorphometric analysis of biopsies from postmenopausal osteoporotic women before and after treatment with PTH have shown significant increases in cancellous bone volume and connectivity with improved trabecular morphology (Jiang *et al.*, 2003). At cortical skeletal sites, PTH does not increase bone density. In fact, there may be a small decline in BMD in association with an increase in cortical porosity due to resorption of fully mineralized endocortical bone. However, this does not result in decreased bone strength because the increased porosity occurs only in the inner one third of bone, where the mechanical stress is minimal. Even more importantly, other salutary effects of teriparatide on cortical bone overcome this increase in cortical porosity. PTH stimulates periosteal apposition, which leads to an increase in cortical area, cortical thickness, and an overall increase in cross-sectional area (Burr *et al.*, 2001). Microarchitectural changes due to teriparatide are evident at the

cortical sites as well. These geometrical and microarchitectural changes strengthen cortical bone despite the small reduction in BMD.

In rodents, a substantial increase in bone mass with PTH administration has been demonstrated in several studies in intact (Mosekilde *et al.*, 1991), sex-hormone-depleted (Andreassen and Oxlund, 2000; Kimmel *et al.*, 1993; Liu *et al.*, 1991), and aged animals (Ejersted *et al.*, 1995; Ejersted *et al.*, 1994). Biomechanical competence has been shown to be increased both in cancellous and cortical bone (Ejersted *et al.*, 1995; Mosekilde *et al.*, 1991). At the tissue level, thickening of trabecular elements has been described (Kneissel *et al.*, 2001; Kimmel *et al.*, 1993). This was explained mainly by an increase in mineralizing surface and some increase in mineral apposition rate, whereas eroded surface and number of osteoclasts remained comparable to control values. Both endocortical and subperiosteal bone formation have been reported to be increased in compact bone, although the anabolic effect was found to be stronger at the endocortical envelope (Ejersted *et al.*, 1994; Andreassen and Oxlund, 2000).

The rationale for considering GH as a potential anabolic agent is that it is critical for the postnatal acquisition and maintenance of bone mass. An added theoretic advantage is salutary effects on muscle strength and coordination. In patients with growth hormone deficiency, replacement of growth hormone increases bone mass. Results from a cross-sectional study indicate that patients with growth hormone deficiency who are receiving growth hormone-replacement therapy have a reduced risk of vertebral fractures as compared with untreated patients (Canalis *et al.*, 2007). Although the beneficial effects of growth hormone on the skeleton appear to be clear in patients with growth hormone deficiency, this is not the case in the absence of growth

hormone deficiency (Canalis *et al.*, 2007). GH increases BMD in patients with postmenopausal osteoporosis, but the effects are inconsistent, and well-designed longitudinal studies showing a reduction in the risk of fracture in this condition with GH have not been reported. The use of growth hormone in osteoporosis is likely to be limited by side effects such as weight gain, carpal tunnel syndrome, glucose intolerance, and edema (Canalis *et al.*, 2007).

The effects of GH on the rat skeleton have been extensively studied. GH administration in both young and old rats has been shown to stimulate cortical bone formation of the femoral diaphysis by an increase in subperiosteal bone formation. (Andreassen *et al.*, 1996; Jorgesen *et al.*, 1991; Mosekilde *et al.*, 1998). Mechanical testing of the femur by three-point bending resulted in increased ultimate load and moment of inertia but did not have an effect on stress or elastic modulus (Mosekilde *et al.*, 1999). Furthermore, the significant increases in femoral strength were only seen at GH doses greater than 2 mg/kg/day (Mosekilde *et al.*, 1998). Histomorphometric studies have shown a limited effect of GH on trabecular bone. Gunness and Hock (1995) demonstrated that GH treatment in intact 18 month-old rats resulted in no significant increase in trabecular bone volume or formation rate. Furthermore, in younger sham rats treated with GH no significant increases were observed in vertebral strength. (Andreassen *et al.*, 1996).

IGF-I is primarily released from the liver into the circulation upon GH stimulation, although it is synthesized by multiple fetal and adult tissues (Tobias *et al.*, 1992). Epiphyseal cartilage responds to IGF-I by increasing DNA, protein, and proteoglycan synthesis to increase the linear growth of long bones (Froesch *et al.*, 1985).

In cultures of bone and osteoblast-like cells, IGF-I stimulates collagen and DNA synthesis (McCarthy *et al.*, 1989b; Hock *et al.*, 1988). Data on IGF-I therapy exist for postmenopausal and young women. IGF-I is theoretically more appealing than GH, because it stimulates bone formation more directly. When elderly women were administered low doses of IGF-I, markers of bone formation were differentially stimulated with only a minimal increase in bone resorption (Ghiron *et al.*, 1995). Similarly, markers of bone formation increased in short-term trials of young women with anorexia nervosa administered IGF-I (Grinspoon *et al.*, 1996). A major drawback to the development of IGF-I as a therapy for osteoporosis is its ubiquitous effect on many organ systems. Like GH, potential serious adverse effects could surface with its chronic use.

Studies of IGF-I in rodent bone show that it has both cortical and trabecular effects. In 4 month-old OVX rats, IGF-I has been found to increase periosteal bone formation at the tibial diaphysis (Tobias *et al.*, 1992). Furthermore, continuous infusion of IGF-I *in vivo* into the rat hindlimb has been shown to stimulate cortical and trabecular bone formation (Spencer *et al.*, 1991). Mueller et al. (1994) have demonstrated that treatment with IGF-I stimulates trabecular bone formation and increases trabecular bone mass in osteopenic adult OVX rats. In addition, IGF-I was reported to prevent trabecular bone loss in adult OVX rats (Kalu *et al.*, 1991)

4.2 Skeletal Effect of AOD

Previously, we have shown that AOD can prevent OVX-induced bone loss and fragility in an aged rat model of postmenopausal osteoporosis (Rowe, 2007). In this study, 9 month-old rats were OVX and treated with AOD for a period of 12 weeks. This was a preventative rather than a recovery study, as OVX was not prolonged before AOD

treatment was initiated. Two doses of AOD were tested for their protective effects against OVX: 0.25 and 0.5 mg/kg/day. Bone quality was assessed using the same methods as in the presented study.

Rowe (2007) found that both doses of AOD increased femoral BMD, femoral cortical thickness, and the strength of cortical bone as evidenced by increased failure torque and energy to failure in torsion, and increased failure load in three-point bending. In trabecular bone, neither dose increased vertebral BMD but 0.25 mg of AOD/kg/day did prevent OVX-induced fragility as evidenced by increased failure stress and energy to failure in vertebral compression. At the structural and material level, this dose attenuated OVX-induced bone loss, increased trabecular bone formation over the sham control, and increased mineralization compared to OVX control. Meanwhile, in trabecular bone 0.5 mg of AOD/kg/day increased stiffness and elastic modulus but did not prevent the OVX-induced deterioration of vertebral mechanical properties. At a structural and material level this was due to an inability to protect against OVX-induced bone loss combined with increases in mineralization over the OVX control. Overall, Rowe (2007) showed that the protective effects of AOD against OVX were more pronounced in cortical than trabecular bone and that these protective effects were more evident at a dose of 0.25 mg/kg/day of AOD.

The two doses used in the study by Rowe (2007) must be considered as part of a spectrum as revealed in a dose study that was performed in parallel. This study looked at the skeletal effects of 0.001, 0.003, 0.01, 0.03, 0.1 and 0.3 mg of AOD/kg/day on 3 month-old OVX rats and revealed that AOD has maximum protective effects against OVX–induced fragility at doses of 0.01 and 0.25 mg/kg/day (unpublished data). The

anabolic ability of AOD was first revealed in an *in vitro* study by Cornish (2002), which showed that AOD significantly stimulated thymidine incorporation (DNA synthesis) and, therefore, proliferation of primary rat osteoblasts. This study demonstrated that AOD has the profile of a bone anabolic, and may have potential as a therapeutic compound in the bone area.

The presented study has shown that AOD treatment given to aged, osteopenic, OVX rats has anabolic and anti-resorptive effects – both with a clear dose-response pattern. In addition, the study has also shown that the effect of AOD treatment is dependent upon the skeletal site investigated.

4.2.1 Anabolic Effect of AOD on Cortical Bone

A cross-sectional analysis of the femoral diaphysis revealed an anabolic effect of AOD on cortical bone. The external anterior/posterior diameter, cortical thickness, cross-sectional area, and moment of inertia of the femoral diaphysis were all significantly increased over both control groups in AOD-0.25. The increase in moment of inertia and cross-sectional area suggests that the new osseous tissue was deposited far from the neutral axis (i.e. the centre of the marrow cavity). Therefore, AOD seems to have increased femoral cortical bone mass mainly though periosteal apposition. Similarly, GH administration in young and old rats has been shown to stimulate cortical bone formation of the diaphysis by an increase in periosteal bone formation (Mosekilde *et al.*, 1998; Andreassen *et al.*, 1996; Jorgesen *et al.*, 1991). Interestingly, although the binding site of AOD is unknown, it has clearly been shown in competition studies that it is not the growth hormone receptor (GHR) (Ogru *et al.*, 2000; Heffernan *et al.*, 2001c; Ng *et al.*,

2000). Nonetheless, AOD appears to have the same downstream anabolic effect as GH on cortical bone.

The mechanism of this anabolic effect remains a matter of speculation. Several experimental findings suggest that IGF-I may be involved. Tobias *et al.* (1992) have found that in 4 month-old OVX rats, IGF-I stimulated periosteal bone formation rate at the tibial diaphysis. This is consistent with a previous observation, which showed that continuous single limb infusions of IGF-I stimulate cortical bone formation in intact adult female rats (Spencer *et al.*, 1991)

IGF-I is primarily released from the liver into the circulation upon GH stimulation, although it is also synthesized by multiple adult tissues (Tobias *et al.*, 1992). In addition, rat osteoblasts have been shown to produce IGF-I with regulation by GH and PTH (McCarthy *et al.*, 1989a). In turn, IGF-I has been shown to regulate bone formation both systemically and locally (Baylink *et al.*, 1993) Furthermore, osteoblastic cells *in vitro* contain receptors for both GH and IGF-I and show increased proliferation in their presence (Barnard *et al.*, 1991). Therefore, it is possible that the GH peptide, AOD, indirectly stimulated hepatic and local osteoblastic IGF-I synthesis, which in turn induced an anabolic effect on cortical bone.

Curiously, the AOD-induced increase in femoral cross-sectional geometry did not lead to a change in mechanical properties except in three-point bending where ultimate stress was significantly decreased in AOD-0.25 compared to both OVX and normal controls. Anabolic therapies such as PTH are known to increase bone turnover substantially, effectively reducing mean tissue age, thus decreasing mineralization, and increasing cortical bone porosity (Turner, 2002). Increases in porosity cause

disproportionate decreases in bone strength, i.e., small increases in porosity can decrease bone strength substantially (Turner, 2002). With PTH treatment in rodents, the increase in porosity does not result in decreased bone strength because the increased porosity occurs mainly in the inner one third of bone, where the mechanical stress is minimal (Turner, 2002). We speculate that with AOD treatment, an increase in porosity throughout the femoral cortex may be decreased femoral strength.

Overall, there is similarity between GH and AOD effects on the cortical skeleton. However, one obvious discrepancy arises in effective doses. Studies in aged OVX rats have shown significant skeletal effects only with growth hormone doses greater than 2 mg/kg/day (Mosekilde *et al.*, 1998; Jorgesen *et al.*, 1991; Andreassen and Oxlund, 2000). Meanwhile, our study and Rowe (2007) have shown similar responses with a much lower dose (0.25 mg/kg/day). Furthermore, previous work from our lab on the skeletal effect of AOD in the OVX rat tested 0.75 mg/kg/day and 2.0 mg/kg/day and found that these doses did not produce significant skeletal effects. Therefore, it appears that the growth hormone peptide, AOD, is more potent than the intact growth hormone. A similar result has also been shown in lipolytic studies in which a lower molar dose of AOD9604 has been to shown to elicit the same lipolytic effect as the intact hGH (Ng *et al.*, 2000).

4.2.2 Anabolic Effect of AOD on Trabecular Bone

Estrogen loss due to OVX induced an elevated cancellous bone turnover in the proximal tibiae of old retired breeder rats as evidenced by a significant increase in osteoid volume (%OV) and osteoid surface (OS/BS) in the OVX group over the normal group. However, with AOD administration, bone turnover began to return to the level of aged estrogen-competent animals after 12 weeks of treatment. In accordance with

previous findings (Miller and Wronski, 1993), substantial progressive cancellous bone loss occurred in the OVX group predominantly by a reduction in trabecular bone volume and number of trabeculae and an increase in trabecular separation. Retired breeders with intact ovaries also showed an age related component of cancellous bone loss. These observed patterns are consistent with the long-term effects of ovariectomy and aging on the rat tibia described by Wronski *et al.* (1989).

Estrogen-deficient animals treated for 12 weeks with AOD showed a dose-dependent increase in trabecular bone volume (%TBV) and trabecular number (Tb.N.) and a dose-dependent decrease in trabecular separation (Tb.Sp.) over the OVX control. This improvement in the architecture of trabecular bone tissue is evidence of the bone-forming effect of AOD. However, while these parameters were significantly restored over the OVX control in AOD-0.25, they were also significantly lower than the normal control indicating that AOD did not fully restore trabecular bone structural properties. This is in contrast to the very pronounced anabolic effect of PTH, which has been shown to restore trabecular bone structural parameters to sham levels in 1 year-old OVX rats with established osteopenia (Kneissel *et al.*, 2001). However, the duration of PTH treatment used by Kneissel *et al.* (2001) was 36 weeks suggesting that in our study, a treatment period of longer than 12 weeks may have fully restored the trabecular architecture of the proximal tibia.

Vertebral compression analysis showed that administration of AOD to aged, osteopenic, OVX rats resulted in restoration of trabecular bone strength; that is, a dose-dependent trend versus the OVX control to increase ultimate stress was evident in AOD-0.25. Similarly, PTH treatment in 1 year-old osteopenic OVX rats has been shown to

increase the biomechanical strength and quality of vertebral bone compared to age matched OVX controls (Mosekilde *et al.*, 1994). The improvement in biomechanical properties with AOD might be ascribed to the improved architecture of cancellous bone tissue.

In cortical bone, our study indicates that AOD appears to have the same downstream actions as GH by inducing pronounced periosteal bone formation at the femoral diaphysis. However, previous histomorphometric studies show a limited effect of GH on trabecular bone. Gunness and Hock (1995) demonstrated that GH treatment in intact 18 month-old rats resulted in no significant increase in trabecular bone volume or formation rate. Furthermore, in younger sham rats treated with GH no significant increases were observed in vertebral strength or trabecular bone volume (Andreassen *et al.*, 1996).

The presented study revealed that AOD has a restorative effect on vertebral strength and trabecular architecture. Previously, we suggested that indirect stimulation of hepatic and osteoblastic IGF-I synthesis by AOD may have been responsible for the pronounced periosteal bone formation at the femoral diaphysis. This indirect stimulation of IGF-I by AOD may have also been responsible for the anabolic effects seen in trabecular bone.

Previous studies confirm the bone-forming effect of IGF-I on trabecular bone. Mueller *et al.* (1994) demonstrated that treatment with IGF-I stimulates trabecular bone formation and increases trabecular bone mass in osteopenic adult OVX rats. This beneficial effect of IGF-I was related to both an increased number of osteoblasts and the synthesis of new bone matrix as evidenced by increased osteoid surface. This anabolic

effect *in vivo* is consistent with the reported stimulatory effects of IGF-I on the proliferation of obsteoblastic cells in culture (Canalis *et al.*, 2007; Barnard *et al.*, 1991). Furthermore, IGF-I was reported to prevent trabecular bone loss in adult OVX rats (Kalu *et al.*, 1991).

4.2.3 Anti-resorptive effect of AOD

Torsion testing revealed a significant increase in stiffness for all three AOD-dosed groups over the OVX and normal controls, which, upon normalization, was preserved in shear modulus. Stiffness and elastic modulus are known to be closely related to the mineralization of bone (Turner and Burr, 2001). Consequently, the increase in these parameters with AOD administration agree with BSE results, which reveal a non-significant shift of 2.3% towards increased mineralization of cortical bone in AOD-0.25.

Vertebral compression results also revealed a dose-dependent increase in stiffness and modulus; an increase that became significant over both control groups at the highest AOD dose. The increase in stiffness and modulus with AOD administration agrees with BSE results, which show a non-significant shift of 2.6% towards increased mineralization of trabecular bone at the highest dose of AOD.

Curiously, skeletal anabolic compounds are known to decrease tissue mineralization by substantially increasing bone turnover and reducing mean tissue age (Turner, 2002). On the other hand, strong inhibitors of bone resorption, such as bisphosphonates, can increase mineralization by reducing bone turnover and increasing mean tissue age (Turner, 2002). PTH was shown to lower the degree of cortical and cancellous bone mineralization in 1 year-old OVX rats with established osteopenia, consistent with the high degree of newly formed unmineralized bone (Kneissel *et al.*,

2001). This is the opposite trend to what was described in minipigs after treatment with alendronate, where bone showed higher mineralization, possibly resulting from lowered bone turnover (Roschger *et al.*, 1997). Therefore, it appears that AOD has a anti-resorptive effect by being able to increase the mineralization of cortical and trabecular bone. Nonetheless, it is important to note that AOD maintained significantly higher bone formation than the normal control indicating that, in addition to having some anti-resorptive capacity, AOD also functions as a compound that is anabolic to bone.

4.3 Methodological Issues

4.3.1 Introduction

There are several limitations to the experimental techniques used to evaluate rodent bone quality. These methodological issues should be taken into consideration when interpreting the results.

4.3.2 Rats

In spite of the increasing use of the ovariectomized rat for studying ovarian hormone deficiency, it has had difficulty in being accepted as an appropriate model of postmenopausal bone loss. The reasons for this are, at least, twofold. First, the rat is often perceived to be growing continuously and has, therefore, been deemed unsuitable as a model of a human disease that starts after the attainment of skeletal maturity. Second, rats appear not to have the same pattern of bone remodeling as humans. These concerns about the rat model merit consideration and are discussed below.

With regard to the widespread notion that the rat skeleton is continuously growing throughout life, there is no doubt that laboratory rats fed ad libitum continue to increase

their body weight for a substantial part of their life span (Yu *et al.*, 1982). Because earlier studies on rats were carried out with young growing animals, this led to the perception that the rat skeleton is also continuously growing. Several observations indicate that this is not so. Yu *et al.* (1982) have demonstrated that in F344 rats, increase in body weight after adulthood is due more to the deposition of fat than to an increase in lean body mass, and that at advanced age rats lose both adiposity and lean body mass. The finding of Kalu *et al.* indicate that the long bones of rats do not grow continuously throughout life (Kalu *et al.*, 1989; Kalu *et al.*, 1984) as the epiphyseal growth plates become sealed off by bone at advanced age (Kalu *et al.*, 1984). These findings are in contradiction to the notion that the rat skeleton is continuously growing throughout life.

The second problem associated with the rat model is the perception that the rat skeleton lacks Haversian systems and does not remodel. This issue is of great significance since the etiology of postmenopausal bone loss may reside in a defect in bone remodeling. In this regard, the studies of Baron *et al.* on bone remodeling in the rat are noteworthy. Baron and his colleagues have demonstrated that the cancellous bone remodeling activities involving the activation (A), resorption (R), and formation (F) phases of a typical bone multicellular unit (BMU) occur at several sites in the rat skeleton, including, cancellous bone in the tail vertebrae (Baron *et al.*, 1984), alveolar bone (Vignery and Baron, 1980) and the mandibular periosteal surface (Tran Van *et al.*, 1982). The remodeling activities at these sites were found to be strikingly similar to those of adult human cancellous bone.

With regard to cortical bone remodeling, rats lack Haversian systems and are thought not to experience intracortical bone remodeling. The adverse effects of this

limitation on data interpretation can be minimized by the use of aged rats with a slowly growing skeleton and/or by restricting data collection to lamellar bone of the vertebral bodies or the secondary spongiosa of long bones (Wronski and Yen, 1991).

4.3.3 Dual Energy X-Ray Absorptiometry (DXA)

While DXA is the most commonly used densitometry approach to measure BMD, an important issue concerning the technique must be addressed. BMD as determined by DXA is a density measurement based on area rather than volume. As such, it is less sensitive to changes in thickness of the specimen (i.e. axis that is parallel to the direction of x-ray projection), since BMD is normalized by the sample area and not entire volume.

According to femoral BMD tests, AOD did not improve cortical bone mineral density despite significant increases in geometrical properties of the femur. This discrepancy may have resulted from an aforementioned limitation of DXA; that is, it is less sensitive to changes in the thickness of a specimen (i.e. axis that is parallel to direction of x-ray projection). Therefore, we did not see an increase in femoral BMD due to the fact that the anterior-posterior diameter of the femur, in which wee saw a significant increase with AOD administration, was parallel to the direction of x-ray projection by the DXA machine.

According to vertebral BMD tests, AOD did not improve trabecular bone mineral density; however, bone quality tests revealed that AOD-0.25 increased mineralization and partially restored the bone lost due to OVX. This discrepancy may have been due to the fact that the non-significant improvements in trabecular mineralization and partial restoration of trabecular bone loss with AOD administration were not pronounced enough to be detected as an increase in BMD by DXA.

4.3.4 Three-Point Bending

The inherent geometry of rat femora presents an issue with using traditional three-point bending. The span of the specimen that is loaded (gauge length) must be sufficiently long to guarantee an accurate test. If the gauge length is very short, most of the displacement induced by loading will be due to shear stresses and not bending (Turner and Burr, 1993). In general, gauge length should be about 16 times the thickness of the specimen (Turner and Burr, 1993). In bending tests of whole bones, unfortunately, a length-to-width ratio of 16:1 cannot be achieved. For long bones, the length-to-width ratio is typically less than half of the recommended value, so shear stresses will cause substantial displacement. These effects cause the measured displacement to be greater than the flexural displacement of the bone, resulting in an overestimation of strain and an underestimation of Young's modulus (Turner and Burr, 2001). With this unavoidable, non-ideal characteristic in mind, three-point bending of whole rat femora is an acceptable and widespread technique used to assess skeletal fragility (Turner and Burr, 1993; Yuehuei *et al.*, 2000; Van der Meulen *et al.*, 2001; Jorgesen *et al.*, 1991; Mosekilde *et al.*, 1998). Moreover, mechanical testing is typically performed to compare relative changes between different experimental groups rather than focusing on the absolute values.

The analysis of three-point bending tests on rat femora also has several inherent assumptions. First, to accurately use the relative normalization formulae (equations 1 and 2, Section 2.5.1), it is assumed that the cortical bone shaft is homogenous in both geometry and intrinsic material properties. Not only does the composite nature of bone result in variations in material properties along the femoral shaft, but the cross-sectional area varies greatly along the femoral shaft as well. While the heterogeneity in material

properties cannot be avoided, it is believed that the particular segment of bone that is tested in three-point bending (15.6 mm centered on midpoint of shaft) has minimal amount of variation in cross-sectional area.

In terms of the actual bone cross-sectional area that is used in the normalization formulae, this section should be as close to the actual fracture site as possible. This is often difficult to achieve, since the fracture is rarely a perfect transversal split. As such, we manually cut the bone shaft close to the fracture site in order to have a complete cross-section. Using an approximate cross-sectional area results in overestimation of some of the normalized mechanical properties. For example, energy to failure should be normalized by the actual uneven surface area of the fracture site, rather than an idealized levelled section (which would subsequently have a smaller surface area) (Walter *et al.*, 1989). However, using a cross-sectional area in close proximity to the actual fracture site is the accepted approach, and is most applicable when comparing differences between experimental groups.

4.3.5 Torsion Testing

Methodological issues concerning torsion testing are largely due to the complicated and time-consuming experimental set-up. First, it is difficult to maintain alignment of the bone sample while its potting material (PMMA) is hardening. While care was taken to continually check alignment in all directions during the setting process, inaccuracies due to limitations of the human eye are inevitable. The use of PMMA as a potting material also presents some inherent issues. It was often difficult to achieve a strong bond between the polymerized PMMA and the actual moist bone surface. As

such, with the onset of torque loading, some initial shifting between the bone and PMMA often occurred, leading to a toe region in the torque-angular displacement curve.

The analysis of torsion curves necessitates many of the same assumptions used in three-point bending. One additional assumption worth mentioning is the use of the contralateral femur (i.e. same cross-sectional area used for three-point bending) for normalization purposes. The nature of the torsion test makes it impossible to generate a useful cross-sectional area of the actual specimen following fracture. However, it has previously been shown that geometrical properties do not significantly differ between left and right femora within the same animal (Battraw *et al.*, 1996). Despite the limitations and assumptions, torsion testing is an accepted and widely used technique for assessment of bone shear properties (Brodt *et al.*, 1999; Turner and Burr, 1993; Rowe, 2007; Yuehuei *et al.*, 2000).

4.3.6 Vertebral Compression

Vertebral compression is a clinically relevant mechanical test; however, the relatively small size of rat vertebrae presents technical challenges. First, the small size creates difficulty in sample preparation, as the spinous processes must be manually cut from the vertebral body. Cutting may create microcracks or defects in the vertebral body that are difficult to observe even under a dissecting microscope. These microcracks would subsequently act as stress concentrators in the vertebral body, leading to a potentially inferior mechanical integrity. Further, the precise set-up of the individual vertebrae in the testing apparatus is often difficult to achieve. Similar to the torsion set-up, PMMA is used to fix the bone in place during the test. Again, difficulties with

bonding between PMMA and the moist vertebra body can exist, which often resulted in shifting of the sample once contact with the lower platen was established.

The analysis of vertebral compression curves also requires a major assumption. The formulae used in normalization of the load-displacement curve (equations 9 and 10, Section 2.5.3) assume that the vertebral body has a solid (rather than porous) structure. Since the actual vertebral body volume is less than that estimated from the digital images, the normalized properties from vertebral compression are underestimations of the true properties. Despite these assumptions, the vertebral compression technique and its normalization procedure is an accepted method in this field of study (Turner and Burr, 1993; Yuehuei *et al.*, 2000; Rowe, 2007; Turner and Burr, 2001; Andreassen *et al.*, 1996).

4.3.7 Femoral Neck Fracture

Methodological issues concerning femoral neck fracture tests are similar to those present in torsion. It was often difficult to ensure exact alignment with the formal shaft in relation to the direction of applied load, as this alignment was validated by the human eye. In addition, similar to both torsion and vertebral compression, an inadequate bond between the potting material (PMMA) and the moist bone sample may have resulted in shifting upon the initial application of load.

While care was taken to minimize flawed tests, variation in measurements was large, especially in the OVX group. As such, we saw a significant increase in ultimate load, failure displacement, and energy to failure in the OVX group over the normal group. Previous studies in aged rats have shown that OVX induces no significant difference in femoral neck strength between OVX and sham animals (Mosekilde *et al.*,

1998; Bagi *et al.*, 1997). This discrepancy may have resulted from an aforementioned limitation of femoral neck fracture; shifting of the sample due to an inadequate bond between the moist bone and PMMA. Such shifting resulted in a large plateau in a number of our load-displacement curves (especially in the OVX group), which lead to an over-estimation of ultimate load, failure displacement, and energy to failure.

Nonetheless, femoral neck fracture is a commonly used clinically-relevant mechanical test, and it is common practice to report the un-normalized (structural) results due to the irregular geometric properties of the femoral neck. (Jamsa *et al.*, 1998; Jamsa *et al.*, 1999; Turner and Burr, 2001).

4.3.8 Histomorphometry and Strut Analysis

While histomorphometry and strut analysis techniques determine bone properties in only two dimensions, this approach has been used in bone research for decades (Parfitt *et al.*, 1987; Revell, 1983). One particular technique difficulty that can affect results is the location at which the 2D section is taken among the bone volume. It is often difficult to ensure that equivalent bone depths within the bone volume are maintained from sample to sample, as the depth is simply verified by visual inspection. While care was taken to compare sample depths, the use of a sufficient sample size again helped decrease the variation in measurements.

Another technique difficulty present in histomorphometry is the identification of eroded surfaces. This was particularly difficult due to fact that, when looking though a microscope, eroded surfaces and bone tissue damage due to sample handing look very similar. Consequently, this resulted in an over-estimation of eroded surfaces.

The area used in both histomorphometric and strut analysis is user defined. As such, some variation may exist in the total tissue area analysed between samples. With histomorphometric measurements, the total tissue area in proximal tibia sections was limited to 8 fields (see Section 2.6.1 for detailed description), originating at a constant length from the outer cortex. With strut analysis, a mask was manually drawn to exclude the outer cortex and growth plate. This manual creation of masks for image analysis has been performed in several studies (Grynpas *et al.*, 1994; Agarwal *et al.*, 2004). While care was taken to ensure consistent criteria were met in drawing each mask, some variation may have occurred. Nonetheless, the masks were consistently drawn by our experienced image analysis, and a sufficient sample size was again used to help decrease any potential variation in measurements.

4.3.9 Microhardness Testing

Another limitation of this study was the discrepancy in mineralization shown through BSE and microhardness tests. While BSE showed decreases in mineralization due to OVX and increases due to AOD treatment, microhardness tests showed no differences in the average hardness of cortical or trabecular bone amongst the five groups. While mineralization is an important determinant of microhardness, other intrinsic properties of bone tissue, such as collagen fiber orientation, may also influence microhardness. Therefore, the discrepancy between our mineralization and microhardness results may be due to the influence of intrinsic factors other than the degree of mineralization on microhardness.

4.4 Conclusions

In the present study, we found that the anabolic effect of AOD was dose-dependent and site-specific. In cortical bone, AOD treatment increased the cross-sectional geometry of the femoral diaphysis via periosteal apposition without much effect on mechanical properties. In trabecular bone, AOD partially restored trabecular architecture, which resulted in an improvement in vertebral mechanical properties. In addition, we have found that AOD increased mineralization as well as stiffness and modulus of cortical and trabecular bone indicating that AOD may also have some anti-resorptive effect in addition to its anabolic effect.

4.5 Future Work

The information gained from this study should be used to develop a follow up study to explore the anabolic effect of AOD on the skeleton more closely. The next study should be improved over the current one by the following suggestions:

Dynamic histomorphometry should be performed in addition to static histomorphometry. This will provide us with a quantitative assessment of the extent of bone formation over a specific period of time. In addition, Calcein Green instead of Oxytetracyline should be administered as the fluorescent marker used to measure bone formation kinetics due to its ability to fluoresce more intensely under ultraviolet light.

Tartrate-Resistant Acid Phosphatase (TRAP) staining staining should be performed in addition to the Goldner's Trichrome stain. Osteoclasts selectively express and stain positive for the TRAP enzyme, providing an index for bone resorption.

Finally, the femoral neck fracture test should be improved by developing different jigs or different sample preparation that will allow less slippage and results with less variability.

References

Agarwal,S., Dumitriu,M., Tomlinson,G., and Grynpas,M. (2004) Medieval trabucular bone architecture: the influence of age, sex, and lifestyle. *American Journal of Physical Anthropology* **124,** 33-44.

Andreassen,T., Melsen,F., and Oxlund,H. (1996) The influence of growth hormone on cancellous and cortical bone on the vertebral body in aged rats. *Journal of Bone and Mineral Research* **11,** 1094-1102.

Andreassen,T. and Oxlund,H. (2000) The influence of combined parrathyroid hormone and growth hormone treatment on cortical bone in aged ovariectomized rats. *Journal of Bone and Mineral Research* **15,** 2266-2275.

Bagi,C., Ammann,P., Rizzoli,R., and Miller,S. (1997) Effect of estrogen deficiency on cancellous and cortical bone structure and strength of the femoral neck in rats. *Calcified Tissue International* **61,** 336-344.

Baker,A., Hollingshead,P., Pitts-Meek,S., and Hansen,S. (1992) Osteoblast-specific expression of growth hormone stimulates bone growth in transgenic mice. *Molecular Cell Biology* **12,** 5541-5547.

Barnard,R., Ng,K., Martin,T., and Walters,M. (1991) Growth hormone receptors in clonal osteoblast-like cells mediate a mitogenic response to GH. *Endocrinology* **128,** 1459-1464.

Baron,R., Tross,R., and Vignery,A. (1984) Evidence of sequential remodeling in rat trabecular bone: morphology, dynamic histomorphometry, and changes during skeletal maturation. *Anatomical Records* **208,** 137-145.

Baroncelli,G., Bertelloni,S., Sodini,F., and Saggese,G. (2003) Acquisition of bone mass in normal individuals and in patients with growth hormone deficiency. *Journal of Pediatric Endocrinology & Metabolism* **16,** 327-335.

Battraw,G., Miera,V., Anderson,P., and Szivek,J. (1996) Bilateral symmetry of biomechanical properties in rat femora. *Journal of Biomedical Materials Research* **32,** 285-288.

Baylink,D., Finkelman,R., and Mohan,S. (1993) Growth factors to stimulate boen formation. *Journal of Bone and Mineral Research* **8,** S564-S572.

Boivin,G., Chavassieux,P., Santora,A., Yates,J., and Meunier,P. (2000) Alendronate increases bone strength by increasing the mean degree of mineralization of bone tissue in osteoporotic women. *Bone* **27,** 687-694.

Bouillon,R. (1991) Growth hormone and bone. *Hormone Research* **36,** 49-55.

Boyde,A. and Jones,S. (1983) Back-scattered electron imaging of skeletal tissues. *Metabolic Bone Diseases and Related Research* **5,** 145-150.

Brodt,M., Ellis,C., and Silva,M. (1999) Growing C57Bl/6 mice increase whole bone mechanical properties by increasing geometric and material properties. *Journal of Bone and Mineral Research* **285,** E454-E459.

Burr,D. (2002) The contribution of the organic matrix to bone's material properties. *Bone* **31,** 8-11.

Burr,D., Hirano,T., Turner,C., Hotchkiss,C., Brommage,R., and Hock,J. (2001) Intermittently administered human parathyroid hormone (1-34) treatment increases intracortical bone turnover and porosite without reducing bone strength in the humerus of ovariectomized cynomolgus monkeys. *Journal of Bone and Mineral Research* **16,** 157-165.

Butler,A. and Le Roith,D. (2001) Control of growth by the somatropic axis: growth hormone and the insulin-like growth factors have related and independent roles. *Annual Review of Physiology* **63,** 141-164.

Canalis,E. (1995) Growth hormone, skeletal growth factors and osteoporosis. *Endocrine Practice* **1,** 39-43.

Canalis,E., Giustina,A., and Bilezikian,J. (2007) Mechanisms of Anabolic Therpaies for Osteoporosis. *New England Journal of Medicine* **357,** 905-916.

Carlstrom,D. (1954) Microhardness measurements on single haversian systems in bone. *Experientia* **10,** 171.

Clark,R. (1997) Growth hormone and insulin-like growth factor 1: new endocrine therapies in cardiology. *Trends in cardiovascular medicine* **7,** 264-268.

Compston,J., Garrahan,N., Croucher,P., Wright,C., and Yamaguchi,K. (1993) Qauntitative analysis of trabecular bone structure. *Bone* **14,** 187-192.

Cornish,J. AOD peptide *in vitro* bone bioactivity report. 2002. University of Auckland, Metabolic Pharmaceuticals Ltd.
Ref Type: Report

Council of the National Osteoporosis Foundation (1996) Guidelines for the early detection of osteoporosis and prediction of fracture risk. *South African Medical Journal* **86,** 1113-1116.

Currey,J. and Brear,K. (1990) Hardness, young's modulus and yield stress in mammalian mineralized tissues. *Journal of Materials Science: Materials in Medicine* **1,** 14-20.

Daughaday,W. and Harvey,S. (1994) Growth hormone action: clinical significance. In *Growth Hormone* (Edited by Harvey,S., Scanes,G., and Daughday,W.) Pp. 475-496. CRC Press, Boca Raton, Florida.

Daughaday,W. and Rotwein,P. (1989) Insulin-like growth factors I and II. Peptide, messenger ribonucleic acid and gene structures, serum and tissue concentrations. *Endocrinology Review* **10,** 68-91.

Eastell,R., Delmas,P., Hodgson,S., Eriksen,E., Mann,K., and Riggs,B. (1988) Bone formation rate in older normal women; concurrent assessment with bone histomorphometry, calcium kinetics, and biochemical markers. *Journal of Clinical Endocrinology and Metabolism* **67,** 741-748.

Ejersted,C., Andreassen,T., Hauge,E., Melsen,F., and Oxlund,H. (1995) Parathyroid hormone (1-34) increases vertebral bone mass, compressive strength and quality in old rats. *Bone* **17,** 507-511.

Ejersted,C., Andreassen,T., Nilsson,M., and Oxlund,H. (1994) Parathyroid hormone (1-34) increases bone formation and strength of cortical bone in aged rats. *European Journal of Endocrinology* **130,** 201-207.

Eriksen,E., Axelrod,D., and Melson,F. (1994) *Bone Histomorphometry*. Raven Press, New York.

Ernst,M. and Froesch,E. (1988) Growth hormone dependent stimulation of osteoblast-like cells in serum-free cultures via local synthesis of insulin-like growth factor-I. *Biochemical and Biophysical Research Communications* **151,** 142-147.

Ernst,M. and Rodan,G. (1990) Increased activity of insulin-like growth factor (IGF) in osteoblastic cells in the presence of growth hormone (GH): positive correlation with the presence of GH-induced IGF binding protein BP-3. *Endocrinology* **127,** 807-814.

Evans,G., Behiri,J., and Bonfield,W. (1990) Microhardness and young's modulus in cortical bone exhibiting a wide range of mineral volume fractions, and in a bone analogue. *Journal of Materials Science: Materials in Medicine* **1,** 38-43.

Fawcett,E. (2004) The Skeletal Effects of a Growth Hormone-Derived Peptide (AOD9604) in the Aged Rat Model of Postmenopausal Osteoporosis. M.Sc. University of Toronto.

Froesch,E., Schmid,C., Schwander,J., and Zapf,J. (1985) Actions of insulin-like growth factors. *Annual Review of Physiology* **47,** 443-467.

Gala,P., Diaz-Curiel,M., de la Piedra,G., Castilla,R., and Torralbo,G. (1998) Bone mass assessment in rats by dual energy X-ray absorptiometry. *The British Journal of Radiology* **71,** 754-758.

Garcia-Barros,M., Devesa,J., and Arce,V. (2000) Proteolytic processing of human growth hormone (GH) by rat tissues in vitro: influence of sex and age. *Journal of Endocrinological Investigation* **23,** 748-754.

Garrahan,N., Mellish,R., and Compston,J. (1986) A new method for the two-dimensional analysis of bone structure in human iliac crest biopsies. *Journal of Microscopy* **142,** 341-349.

Ghiron,L., Thompson,J., Holloway,L., Hintz,R., Butterfield,G., Hoffman,A., and Marcus,R. (1995) Effects of recombinant insulin-like growth factor I and growth hormone on bone turnover in elderly women. *Journal of Bone and Mineral Research* **10,** 1844-1852.

Griffin,M., Kimble,R., Hopfer,W., and Pacifici,R. (1993) Dual-energy x-ray absorptiometry of the rat:accuracy, precision, and measurement of bone loss. *Journal of Bone and Mineral Research* **8,** 795-800.

Grinspoon,S., Baum,H., Lee,K., Anderson,E., Herzog,D., and Klibanski,A. (1996) Effects of short-term recombinant human insulin-like growth factor I administration on bone turnover in osteopenic women with anorexia nervosa. *Journal of Clinical Endocrinology and Metabolism* **81,** 3864-3870.

Grynpas,M., Kasra,M., Dumitriu,M., Nespeca,R., Very,J., and Mertz,B. (1994) Recovery from pamidronate (ADP): a two-year study in the dog. *Calcified Tissue International* **55,** 288-294.

Grynpas,M. (1993) Age and disease-related changes in the mineral of bone. *Calcified Tissue International* **53,** S57-S64.

Grynpas,M., Chachra,D., and Lundon,K. (2000) Bone Quality in Animal Models of Osteoporosis. *Drug Development Research* **49,** 146-158.

Gunness,M. and Hock,J. (1995) Anabolic effect of parathyroid hormone is not modified by supplementation with insulin-like growth factor I (IGF-I) or growth hormone in aged female rats fed an energy-restricted or ad libitum diet. *Bone* **16,** 199-207.

Harris,W. and Heaney,R. (1969) Effect of growth hormone on skeletal mass in adult dogs. *Nature* **223,** 403-404.

Heaney,R. (1993) Is There a Role for Bone Quality in Fragility Fractures? *Calcified Tissue International* **53,** S3-S6.

Heffernan,M., Summers,R., Thorburn,A., Ogru,E., Gianello,R., Jiang,W., and Ng,F. (2001a) The effect of human GH and its lipolytic fragment (AOD9604) on lipid metabolism following chronic treatment in obese mice and $\beta_{3\ \text{knock-out mice}}$. *Endocrinology* **142,** 5182-5189.

Heffernan,M., Thorburn,A., Fam,B., Summers,R., Conway-Campbell,B., Waters,M., and Ng,F. (2001b) Increase of fat oxidation and weight loss in obese mice caused by chronic treatment with human growth hormone or a modified C-terminal fragment. *International Journal of Obesity* **25,** 1442-1449.

Heffernan,M., Summers,R., Thorburn,A.W., Ogru,E., Gianello,R., Jiang,W.J., and Ng,F. (2001c) The effect of human GH and its lipolytic fragment (AOD9604) on lipid metabolism following chronic treatment in obese mice and $\beta_{3\text{-AR knock-out mice}}$. *Endocrinology* **142,** 5182-5189.

Heffernan,M., Jiang,W., Thorburn,A., and Ng,F. (2000) Effects of oral administration of a sythetic fragment of human growth hormone on lipid metabolism. *American Journal of Physiology - Endocrinology and Metabolism* **279,** E501-E507.

Hock,J., Centrella,M., and Canalis,E. (1988) Insulin-like growth factor has independent effect on bone matrix formation and cell replication. *Endocrinology* **122,** 254-260.

Huja,S., Katona,T., and Roberts,W. (2001) Microhardness Testing of Bone. In *Bone Mechanics Handbook* (Edited by Cowin,S.) Pp. 247-254. CRC Press LLC, Boca Raton, Florida.

Inzycchi,S. and Robbins,R. (1994) Effects of growth hormone on human bone biology. *Journal of Clinical Endocrinology and Metabolism* **79,** 691-694.

Isaksson,O., Lindahl,A., Nilsson,A., and Isagaard,J. (1987) Mechanism of the stimulatory effect of growth hormone on longitudinal bone growth. *Endocrinology Review* **8,** 426-438.

Isgaard,J., Nilsson,A., Lindahl,A., Jansson,J., and Isaksson,O. (1986) Effect of local administration of GH and IGF-I on longitudinal bone growth in rats. *American Journal of Physiology* **250,** E367-E372.

Jamsa,T., Koivukangas,A., Ryhanen,J., Jalovaara,P., and Tuukkanen,J. (1999) Femoral neck strength is a sensitive indicator of bone loss in immobilized hind limb of mouse. *Journal of Bone and Mineral Research* **14,** 1708-1713.

Jamsa,T., Tuukkanen,J., and Jalovaara,P. (1998) Femoral neck strength of mouse in two loading configurations: method evaluation and fracture characteristics. *Journal of Biomechanics* **31,** 723-729.

Jee,W. (2001) Integrated Bone Tissue Physiology: Anatomy and Physiology. In *Bone Mechanics Handbook* (Edited by Stephen C.Cowin) Pp. 1-68. CRC Press LLC, Boca Raton, Florida.

Jepsen,K., Akkus,O., Majeska,R., and Nadeau,J. (2003) Hierarchical relationship between bone trains and mechanical properties in inbred mice. *Mammalian Genome* **14,** 97-104.

Jiang,Y., Zhao,J., Mitlak,B., Wang,O., Genant,H., and Eriksen,E. (2003) Recombinant human parathyroid hormone (1-34) [teriparatide] improved both cortical and cancellous bone structure. *Journal of Bone and Mineral Research* **18,** 1932-1941.

Jorgesen,P., Bak,B., and Andreassen,T. (1991) Mechanical properties and biochemical composition of rat cortical femur and tibia after long-term treatment with biosynthetic human growth hormone. *Bone* **12,** 353-359.

Kalu,D. (1991) The ovariectomized rat model of postmenopausal bone loss. *Bone and Mineral* **15,** 175-192.

Kalu,D., Hardin,R., Cockerham,R., and Yu,B. (1984) Aging an dietary modulation of rat skeleton and parathyroid hormone. *Endocrinology* **115,** 1239-1247.

Kalu,D., Liu,C., Hardin,R., and Hollis,B. (1989) The aged rat model of ovarian hormone deficiency bone loss. *Endocrinology* **124,** 7-16.

Kalu,D., Liu,C., Salerno,E., Salih,M., Echon,R., Ray,M., and Hollis,B. (1991) Insulin-like growth factor-I partially prevents ovariectomy-induced bone loss: a comparative study with human parathyroid hormone(1-38). *Journal of Bone and Mineral Research* **6,** S221.

Kaplan,F., Hayes,W., Keaveny,T., Boskey,A., Einhorn,T., and Iannotti,J. (1994) Form and Function of Bone. In *Orthopaedic Basic Science* (Edited by Simon,S.R.) Pp. 127-184. American Academy of Orthopaedic Surgeons.

Kato,J., Murakami,Y., Sohmiya,M., and Nishiki,M. (2002) Regulation of Human Growth Hormone Secretion and Its Secretion. *Internal Medicine* **41,** 7-13.

Kimmel,D., Bozzato,R., Kronis,K., Coble,T., Sindrey,D., Kwong,P., and Recker,R. (1993) The effect of recombinant human (1-84) or synthetic human (1-34) parathyroid hormone on the skeleton of adult osteopenic ovariectomized rats. *Endocrinology* **132,** 1577-1584.

Kimmel,D., Recker,R., Gallagher,J., Vaswani,A., and Aloia,J. (1990) A comparison of iliac bone histomorphometric data in post-menopausal osteoporotic and normal subjects. *Bone and Mineral* **11,** 217-235.

Kinney,J., Ryaby,J., Haupt,D., and Lane,N. (1998) Three-dimensional in vivo morphometry of trabecular bone in the OVX rat model of osteoporosis. *Technology and Health Care* **6,** 339-350.

Kneissel,M., Boyde,A., and Gasser,J. (2001) Bone Tissue and its Mineralization in Aged Estrogen-Depleted Rats After Long-term Intermittent Treatment with Parathyroid Hormone (PTH) Analog SDZ PTS 893 or Human PTH(1-34). *Bone* **28,** 237-250.

Lane,N., Haupt,D., Kimmel,D., Modin,G., and Kinney,J. (1999) Early estrogen replacement therapy reverses the rapid loss of trabecular bone volume and prevents

further deterioration of connectivity in the rat. *Journal of Bone and Mineral Research* **14,** 206-214.

Liu,C., Kalu,D., Salerno,E., Echon,R., Hollis,B., and Ray,M. (1991) Preexisting bone oss associated with ovariectomy in rats is reversed by parathyroid hormone. *Journal of Bone and Mineral Research* **6,** 1071-1080.

Lundon,K., Dumitrium,M., and Grynpas,M. (1994) The long-term effect of ovariectomy on the quality and quantity of cancellous bone in young macaques. *Bone and Mineral* **24,** 135-149.

MacDonald,S., Reeder,B., Chen,Y., and Depres,J. (1997) Obesity in Canada: A descriptive analysis. *Canadian Medical Association Journal* **145,** S39-S45.

Marcus,R. (1997) Skeletal effects of growth hormone in IGF-I in adults. *Hormone Research* **48,** 60-64.

Marx,J. (1980) Osteoporosis: New Help for Thinning Bones. *Science* **207,** 628-630.

McCalden,R., McGeough,J., and Court-Brown,C. (1997) Age-related changed in the compressive strength of cancellous bone. The relative importance of changes in density and trabecular architecture. *Journal of Bone and Joint Surgery.American Edition* **79,** 421-427.

McCarthy,T., Centrella,M., and Canalis,E. (1989a) Parathyroid hormone enhances the transcript and polypeptide levels of insulin-like growth factor I in osteoblast-enriched cultures from fetal rat bone. *Endocrinology* **124,** 1247-1253.

McCarthy,T., Centrella,M., and Canalis,E. (1989b) Regulatory effects of insulin-like growth factors I and II on bone collagen synthesis in rat calvarial cultures. *Endocrinology* **124,** 301-309.

Melton,L.I., Kan,S., Frye,M., Wahner,H., O'Fallon,W., and Riggs,B. (1989) Epidemiology of vertebral fractures in women. *American Journal of Epidemiology* **129,** 1000-1011.

Meunier,P. (2001) Anabolic agents for treating postmenopausal osteoporosis. *Joint Bone Spine* **68,** 576-581.

Miller,S. and Wronski,T. (1993) Long-term osteopenic changes in cancellous bone structure in ovariectomized rats. *Anatomical Records* **236,** 433-441.

Mohan,S., Strong,D., Lempert,U., Tremollieres,F., Wergedal,J., and Baylink,D. (1992) Studies on regulation of insulin-like growth factor binding protein (IGFBP)-3 and IGFBP-4 production in human bone cells. *Acta endocrinologica* **127,** 555-564.

Monson,J., Drake,W., Carroll,P., Weaver,J., Rodriguez-Arnao,J., and Savage,M. (2002) Influence of growth hormone on accretion of bone mass. *Hormone Research* **58 Supp 1,** 52-56.

Mosekilde,L., Danielsen,C., and Gasser,J. (1994) The effect of vertebral bone mass and strength of long term treatment with anitresorptive agents (estrogen and calcitonin), human parathyroid hormone (1-38), and combination therapy, assessed in aged, ovariectomized rats. *Endocrinology* **134,** 2126-2134.

Mosekilde,L., Sogaard,C., Danielsen,C., and Torring,O. (1991) The anabolic effects of human parathyroid hormone (hPTH) on rat vertebral body mass are also reflected in the quality of bone, assessed by biomechanical testing. *Endocrinology* **129,** 421-428.

Mosekilde,L., Thomsen,J., Orhii,P., and Kalu,D. (1998) Growth hormone increases vertebral and femoral boen strength in osteopenic, ovariectomized, aged rats in a dose-dependent and site-specific manner. *Bone* **23,** 343-352.

Mosekilde,L., Thomsen,J., Orhii,P., McCarter,R., Mejia,W., and Kalu,D. (1999) Additive effect of voluntary exercise and growth hormone treatment on bone strength assessed at four different skeletal sites in an aged rat model. *Bone* **24,** 71-80.

Mueller,K., Cortesi,R., Modrowski,D., and Marie,P. (1994) Stimulation of trabecular bone formation by insulin-like growth factor I in adult ovariectomized rats. *American Journal of Physiology - Endocrinology and Metabolism* **267,** E1-E6.

Nagy,T., Prince,C., and Li,J. (2001) Validation of peripheral dual-energy X-ray absorptiometry for the measurement of bone mineral in intact and excised long bones of rats. *Journal of Bone and Mineral Research* **16,** 1682-1687.

Natera,S., Jiang,W., and Ng,F. (1994) Reduction of cumulative body weight gain and adipose tissue mass in obese mice: response to chronic treatment with synthetic hGH177-191 peptide. *Biochemistry and Molecular Biology International* **33,** 1011-1021.

Ng,F., Adamafio,N., and Graystone,J. (1990) Effects of exogenous growth hormone on lipid metabolism in the isolated epididymal fat pad of the growth hormone-deficient little mouse. *Journal of Molecular Endocrinology* **4,** 43-49.

Ng,F., Sun,J., Sharma,L., Libinaka,R., Jiang,W., and Gianello,R. (2000) Metabolic studies of a synthetic lipolytic domain (AOD9604) of human growth hormone. *Hormone Research* **53,** 274-278.

Nilsson,A., Swolin,D., Enerback,S., and Ohlsson,C. (1995) Expression of functional growth hormone receptors in cultured human osteoblast-like cells. *Journal of Clinical Endocrinology and Metabolism* **80,** 3483-3488.

Nishiyama,K., Sugimoto,T., Kaji,H., Kantani,M., Kobayashi,T., and Chihara,K. (1996) Stimulatory effect of growth hormone on bone resorption and osteoclast differentiation. *Endocrinology* **137,** 35-41.

Ogru,E., Wilson,J., Heffernan,M., Jiang,W., Chalmers,D., Libinaki,R., and Ng,F. (2000) The conformational and biological analysis of a cyclic anti-obesity peptide from the C-terminal domain of human growth hormone. *Journal of Peptide Research* **56,** 388-397.

Orgu,E., Wilson,J.C., Heffernan,M., Jiang,W.-J., Chalmers,D.K., Libinaki,R., and Ng,F. (2000) The conformational and biological analysis of a cyclic anti-obesity peptide from the C-terminal domain of human growth hormone. *Journal of Peptide Research* **56,** 388-397.

Ott,S. (1993) When bone mass fails to predict bone failure. *Calcified Tissue International* **53,** S7-S13.

Parfitt,A. (1987) Trabecular bone architecture in the pathogenesis and prevention of fracture. *American Journal of Medicine* **82,** 68-72.

Parfitt,M., Drezner,M., Glorieux,F., Kanis,J., Malluche,H., Meunier,P., Ott,S., and Recker,R. (1987) Bone histomorphometry: standardization of nomenclature, symbols, and units. *Journal of Bone and Mineral Research* **2,** 595-610.

Pietrobelli,A., Formica,C., Wang,Z., and Heymsfield,S. (1996) Dual-energy X-ray absorptiometry body composition model; review of physical concepts. *American Journal of Physiology - Endocrinology and Metabolism* **271,** E941-E951.

Reid,S. and Boyde,A. (1987) Changes in the mineral density distribution in human bone with age: image analysis using backscattered electrons in the SEM. *Journal of Bone and Mineral Research* **2,** 13-22.

Revell,P. (1983) Histomorphometry of Bone. *Journal of Clinical Pathology* **36,** 1323-1331.

Rho,J., Kuhn-Spearing,L., and Zioupos,P. (1998) Mechanical properties and the hierarchical structure of bone. *Medical Engineering and Physics* **20,** 92-102.

Roschger,P., Fratzl,P., Klaushofer,K., and Eschberger,J. (1997) Mineralisation of cancellous bone after alendronate and sodium flouride treatment: A quantitative backscattered electron imaging study on minipig ribs. *Bone* **20,** 393-397.

Rowe,E. (2007) Can a growth hormone-derived peptide (AOD9604) prevent bone loss and fragility in a rat model of osteoporosis? M.Sc. University of Toronto.

Saggese,G., Baroncelli,G., Bertelloni,S., Cinequanta,L., and DiNero,G. (1993) Effects of long term treatment with growth hormone in bone and mineral development in children wiht growth hormone deficiency. *Journal of Pediatrics* **122,** 37-45.

Sato,M., McClintock,C., Kim,J., Turner,C., Bryant,H., Magee,D., and Slemenda,C. (1994) Dual-energy x-ray absorptiometry of raloxifene effects on the lumbar vertebrae and femora of ovariectomized rats. *Journal of Bone and Mineral Research* **9,** 715-724.

Scanes,C. and Campell,R. (1995) Growth Hormone: Chemistry. In *Growth Hormone* Pp. 1-23. CRC Press.

Schenk,R., Olah,A., and Herrmann,W. (1994) Preparation of calcified tissues for light microscopy. In *Methods of Calcified Tissue Preparation* (Edited by Dickson,G.) Pp. 1-56. Elsevier, New York.

Schmid,C., Schlapfer,I., Peter,M., Boni-Schnetzler,M., Schwander,J., Zapf,J., and Froesch,E. (1994) Growth hormone and parathyroid hormone stimulate IGFBP-3 in rat osteoblasts. *American Journal of Physiology* **267,** E226-E233.

Sinha,Y. and Jacobsen,B. (1994) Human growth hormone (hGH)-(44-191), a reportedly diabetogenic fragment of hGH, circulates in human blood: measurement by radioimmunoassay. *Journal of Clinical Endocrinology and Metabolism* **78,** 1411-1418.

Spencer,E., Liu,C., Si,E., and Howard,G. (1991) In Vivo Actions of Insulin-Like Growth Factor I (IGF-I) on Bone Formation and Resorption in Rats. *Bone* **12,** 21-26.

Tai,P., Liao,J., Chen,E., Dietz,J., Schwards,J., and Carter-Su,C. (1990) Differential regulation of two glucose transporters by chronic growth hormone treatment of cultured 3T3-F442A adipose cells. *Journal of Biological Chemistry* **265,** 21828-21834.

Tobias,J., Chow,J., and Chambers,T. (1992) Opposite Effects of Insulin-Like Growth Factor I on the Formation of Trabecular and Cortical Bone in Adult Female Rate. *Endocrinology* **131,** 2387-2392.

Tran Van,P., Vignerry,A., and Baron,R. (1982) Cellular kinetics of the bone remodeling sequence in the rat. *Anatomical Records* **202,** 445-451.

Turner,C. (2002) Biomechanics of Bone: Determinants of Skeletal Fragility and Bone Quality. *Osteoporosis International* **13,** 97-104.

Turner,C. and Burr,D. (1993) Basic biomechanical measurements of bone: a tutorial. *Bone* **14,** 595-608.

Turner,C. and Burr,D. (2001) Experimental techiques for bone mechanics. In *Bone Mechanics Handbook* (Edited by Cowin,S.) Pp. 1-17. CRC Press LLC, Boca Raton, Florida.

Ultsch,M., Somers,W., Kossiakoff,A., and de Vos,A. (1994) The crystal structure of affinity-matured human growth hormone at 2 angstrom resolution. *Journal of Molecular Biology* **236,** 286-299.

Van der Meulen,M., Jepsen,K., and Mikic,B. (2001) Understanding Bone Strength: Size Isn't Everything. *Bone* **29,** 101-104.

Verhaeghe,J., van Bree,R., Van Herck,E., Thomas,H., Skottner,A., Dequeker,J., Mosekilde,L., Einhorn,T., and Bouillon,R. (1996) Effects of recombinant human growth

hormone and insulin-like growth factor-I, with or without 17 beta-estradiol, on bone and mineral homeostasis of aged ovariectomized rats. *Journal of Bone and Mineral Research* **11,** 1723-1735.

Vignery,A. and Baron,R. (1980) Dynamic histomorphometry of alveolar bone remodeling in adult rat. *Anatomical Records* **196,** 191-200.

Walter,K., Carlsson,L., Smiley,A., and Gillespie Jr,J. (1989) Mechanisms for rate effects on interlaminar fracture toughness of carbon/epoxy and carbon/PEEK composites. *Journal of Materials Science* **24,** 3387-3398.

Wang,L., Orhii,P., Banu,J., and Kalu,D. (2001) Bone anabolic effects of separate and combined therapy with growth hormone and parathyroid hormone on femoral neck in aged ovariectomized osteopenic rats. *Mechanisms of Ageing and Development* **122,** 89-104.

Wells,J. and de Vos,A. (1993) Structure and function of human growth hormone; implications for the hematopoietins. *Annual Review of Biophysics and Biomolecular Structure* **22,** 329-351.

Wijaya,E. and Ng,F. (1993) Effect of an antilipogenic fragment of human growth hormone on glucose transport in rat adipocytes. *Biochemistry & Molecular Biology International* **31,** 543-552.

Wronski,T., Dann,L., Scott,K., and Cintron,M. (1989) Long-term effect of ovariectomy and aging on the rat skeleton. *Calcified Tissue International* **45,** 360-366.

Wronski,T. and Yen,C. (1991) The ovariectomized rat as an animal model for postmenopausal bone loss. *Cell and Materials* **Supplement 1,** 69-74.

Wu,Z. and Ng,F. (1993) Antilipogenic action of synthetic C-terminal sequence 177-191 of human growth hormone. *Biochemistry & Molecular Biology International* **30,** 187-196.

Yu,B., Masoro,E., Murata,I., Bertrand,H., and Lynd,F. (1982) LIfe span study for SPF Fischer 344 male rats fed ad libitum or restricted diets: longevity, growth, lean body mass and disease. *Journal of Gerontology* **37,** 130-141.

Yuehuei,H., Barfield,W., and Draughn,R. (2000) Basic Concepts of Mechanical Propertry Measurement and Bone Biomechanics. In *Mechanical Testing of Bone and the Bone-Implant Interface* (Edited by Yuehuei,H. and Draughn,R.) Pp. 23-36. CRC Press LLC, Boca Raton, Florida.